LUT UNIVERSITY
LUT School of Energy Systems
LUT Mechanical Engineering
BK10A0402 Kandidaatintyö

UTILIZATION OF WHOLE BUILD VOLUME IN LASER-BASED POWDER BED FUSION

KOKO KAMMIOTILAVUUDEN HYÖDYNTÄMINEN METALLIEN JAUHEPETITEKNIIKASSA

Lappeenranta 28.9.2020
Jouni Rahikainen
Examiner Professor Heidi Piili, D.Sc.(Tech.)
Advisor Project researcher Niko Riikonen, M.Sc.

TIIVISTELMÄ

LUT-Yliopisto
LUT School of Energy Systems
LUT Kone

Jouni Rahikainen

Koko kammiotilavuuden hyödyntäminen metallien jauhepetitekniikassa

Kandidaatintyö

2020

48 sivua, 28 kuvaa, 3 taulukkoa ja 2 liitettä

Tarkastaja: Professori Heidi Piili, TkT

Ohjaaja: Projektitutkija Niko Riikonen, DI

Hakusanat: L-PBF, Lisäävä valmistus, muodonmuutos, huokoisuus, jäännösjännitys, simulaatio, vertikaalinen sijoittelu, sijoittelu

Metallien 3D-tulostaminen on kerännyt huomiota viimeisten vuosien aikana. Kirjallisuutta on kuitenkin kirjoitettu rajallisesti kyseisestä aihepiiristä. Julkaisujen määrä vertikaalisesta sijoittelusta on rajallinen. Valmistusvirheiden muodostumisesta on olemassa tieteellisiä artikkeleita, mutta toistaiseksi 3D-tulostuksen koko tulostustilavuuden hyödyntämisestä ei ole olemassa ohjeistusta tai muita tutkimuksia viimeisen kymmenen vuoden ajalta. Muutoin kirjallisuus antaa hyvät ohjeet metallien 3D-tulostukseen jauhepetitekniikalla. Erityisesti huokoisuuteen ja lämmön johtumiseen on kiinnitetty runsaasti huomiota.

Tässä työssä koko tulostustilavuuden hyödyntämistä kokeiltiin simuloiden käyttämällä Dassault Systémes 3D-Experience ohjelmaa. Simulaatioiden tulokset osoittavat, että jännitykset lisääntyvät, kun rakennettavia kappaleita rakennetaan päällekkäin. Simuloitavia kappaleita olivat vetokoekappale, sekä puolikaaren muotoinen kappale. Molempia kappaleita simuloitiin yksittäin, kahden kerroksissa ja kolmen kerroksissa.

Vetokoekappaleilla oli melko lineaarinen muodonmuutoksen lisääntyminen kappalekerroksien lisääntyessä. Tukirakenteiden murtumista havaittiin useamman kerroksen rakenteissa. Puolikaarille muodonmuutos ei ollut lineaarista kappalekerroksien lisääntyessä. Kaksinkertaisessa rakenteessa esiintyi enemmän muodonmuutosta kuin kolminkertaisessa rakenteessa. Molemmissa kappaletyypeissä oli huomattavia jälkijännityksiä, mutta kappaleissa ei havaittu murtumia.

Vaikka simulaatiotuloksilla oli eroavaisuuksia, jotka perustuivat geometrisiin, sekä dimensionaalisiin eroihin, niin simulaatiotulokset osoittavat, että 3D-tulostettujen rakenteiden tulostaminen päällekkäin on mahdollista, mikäli valmistusvirheiden muodostuminen otetaan huomioon. Aihealue vaatii enemmän tutkimusta, ennen kuin 3D-

tulostettujen rakenteiden tulostamisesta voidaan tehdä yleistä. Tällä hetkellä rakenteiden tulostaminen päällekkäin perustuu laajalti suunnittelijan taitoihin ja kokemukseen.

ABSTRACT

LUT University
LUT School of Energy Systems
LUT Mechanical Engineering

Jouni Rahikainen

Utilization of whole build volume in laser-based powder bed fusion

Bachelor's thesis

2020

48 pages, 28 figures, 3 tables and 2 appendices

Examiner: Professor Heidi Piili

Advisor: Project researcher Niko Riikonen

Keywords: L-PBF, Additive manufacturing, deformation, porosity, residual stress, simulation, vertical stacking, nesting

Additive manufacturing of metals using laser-based powder bed fusion of metals is a manufacturing method that has gained a lot of attention in the recent years. Literature about utilizing the whole build volume in laser-based powder bed fusion of metals is very limited. Literary sources are good in describing defect formation in additive manufacturing, but so far, no guidelines have been published specifically about vertical stacking. Otherwise the literary sources provide a good basis for printing in laser-based powder bed fusion of metals. Porosity and heat conduction have received significant attention in literature.

Vertical stacking of builds is experimented in this bachelor's thesis by done simulations using in Dassault Systémes 3D-Experience. The simulation results show that displacements and stresses increased when builds are stacked. A tensile test rod and a half-arc were simulated as a single build, a double stacked build, and a triple stacked build.

The rods had fairly linear increase in displacement as more builds were added on top. Some cracking was noticed in the supports of the stacked rods. The half-arcs did not have a linear displacement increase in the stacks. Double stacked half-arc had more displacement than the triple stacked build. Both build types had significant stresses, but no cracking was noticed in the parts themselves.

While the results have some differences based on geometrical and dimensional differences, but both show that stacking seems viable if defect formation is taken into account by the designer. More research is required until stacking can be made commonly used in L-PBF as currently the manufacturing results largely depend on the skills and experience of the manufacturer.

TABLE OF CONTENTS

APPENDICES

LIST OF SYMBOLS AND ABBREVIATIONS

AM	Additive manufacturing
FE	Finite element
FEA	Finite element analysis
HIP	Hot isostatic pressing
L-PBF	Laser-based powder bed fusion
PBF	Powder bed fusion
VED	Volume energy density

1 INTRODUCTION

Laser-based powder bed fusion (L-PBF) for metal materials is one additive manufacturing (AM) technique in which an object is manufactured by melting a thin layer of metal powder using a heat source, usually laser, one layer at a time on top of each other. After melting desired sections of the layer, a new powder layer is spread, and this process is repeated until the geometry of the part is completed. (Yang et al. 2017, p. 21; Masoomi et al. 2017, p. 1-3.) Figure 1 visualizes the L-PBF process (Kokkonen et al. 2016, p. 9).

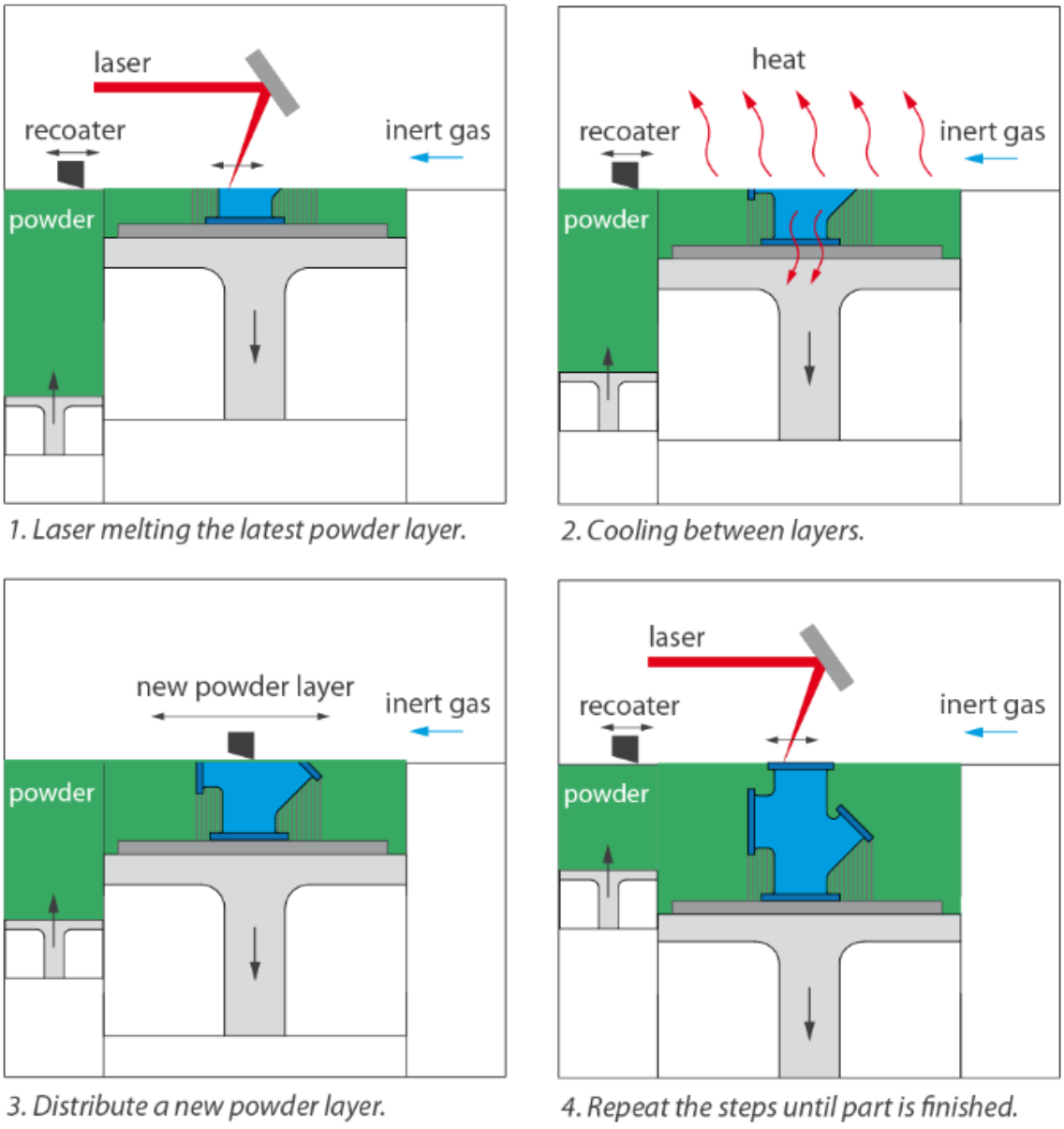

Figure 1. Basic principle of L-PBF (Kokkonen et al. 2016, p. 9)

The L-PBF process is shown in Figure 1 (Kokkonen et al. 2016, p. 9). The powder that has not been melted is left as powder in the previous layers as a base that supports the new layers of powder, not to be confused with supports that are needed for overhangs. The melted powder becomes the fabricated part and works as a support for new layers. (Yang et al. 2017, p. 21.)

1.1 Background

Low productivity and high costs are considered problematic in metal PBF technology. One way to improve productivity is to utilize more of the build chamber volume. A single build may only use a small volume of the building chamber. Nesting, which is the act of placing multiple builds on the build floor, is often done horizontally along the build chamber floor to increase the number of objects being built at once. So far, the vertical direction has mostly been unutilized. In this thesis, nesting vertically is referred to as vertical stacking or stacking. At the time of writing only a few commercial applications in nesting vertically have been made by Etteplan and Betatype. In both cases the improvement of production quantity was one of the driving factors in choosing vertical stacking. Etteplan was able to reduce manufacturing costs by 40 % in their study. (Additive Manufacturing Today 2019; Etteplan 2019.)

1.2 Motivation, research problem and research questions

Even when multiple objects are built at the same time, the whole vertical build volume is not usually used. Current L-PBF machines can utilize the whole build chamber, but the effects of stacking on part quality are mostly unknown. The research questions of this thesis are:

- What are the causes of manufacturing errors in L-PBF when utilizing whole build volume and why?
- How does vertical stacking influence displacements and stresses?
- Which manufacturing errors can be prevented with parameter optimization?
- How build geometry should be taken into consideration when stacking?

Manufacturing errors, also called build errors are the main interests in this research. The effect that stacking has on build error formation is largely unknown as there is not much research done on stacking. Build errors can include, but are not limited to:

1) Distortion of geometry
2) Porosity
3) Residual stresses
4) Thermal expansion.

This thesis was executed as part of project “Metal 3D Innovations (Me3DI)”. Aim of Metal 3D Innovations (Me3DI) project is to form industrial knowhow cluster of metallic 3D printing to South Karelia. This cluster will enhance utilization of AM (3D printing) of metallic materials. The project duration is 1.9.2018-31.12.2020 and is funded by European Regional Development Fund. Cluster for metallic 3D printing gathers regional knowhow in industrial manufacturing and design and utilizes resources of academic research and education at LUT University (LUT). Thesis was written in Lappeenranta, Finland.

1.3 Objective

Through use of simulation this thesis aims to identify effects on build quality when utilizing whole build volume. By identifying the problems and their causes, these aspects can be taken into consideration when manufacturing stacked parts thus improving the overall quality of the builds. Knowledge of the manufacturing defects and how they are formed is critical in optimizing any manufacturing processes for production.

1.4 Scope

Since the field is young and evolves fast it is necessary to use up to date information. Most publications that have been published before 2015 are dismissed as potentially out of date. There is not much research done in vertical stacking. Figure 2 shows results for searching stacked AM research from Scopus.

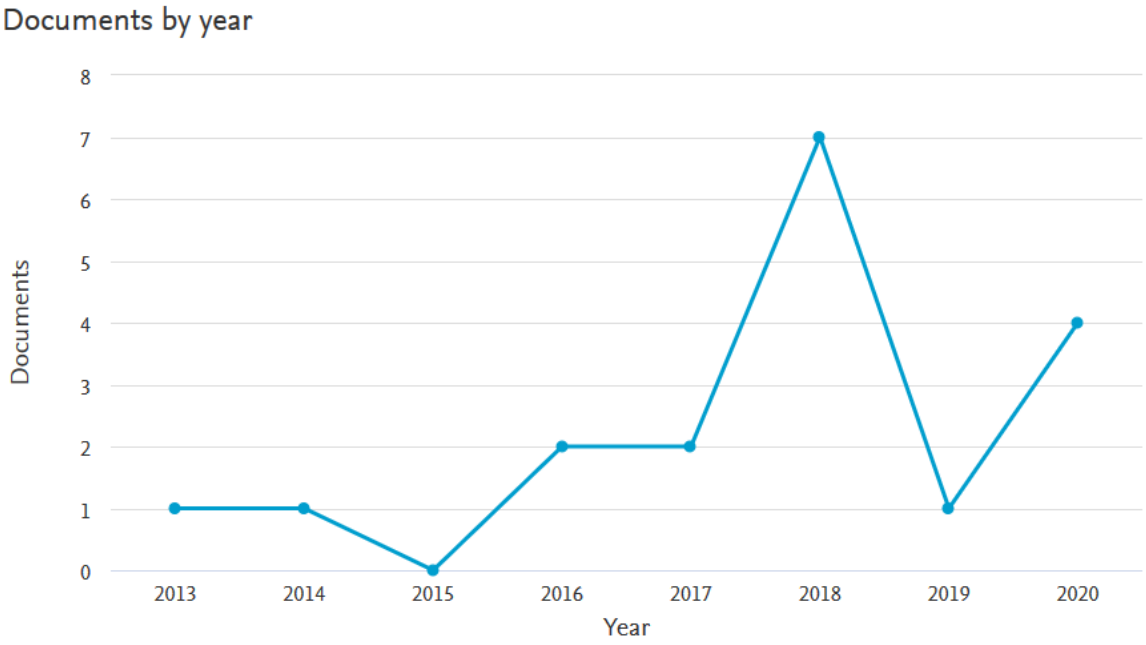

Figure 2. Scopus search results with keywords "additive, manufacturing, nesting" on 16.9.2020.

As seen from Figure 2, there is very little research done on this subject. There are 18 results overall with search “additive, manufacturing, nesting” on 16.9.2020. Although the contents of every publication have not been checked, not all of these results contain information about vertical stacking. Other searches with the keywords “additive, manufacturing, stacking” yielded either no results or no relevant results. 2013 is the first year of occurrence when AM and nesting have been mentioned within Scopus with these words. There is a large decrease of published articles in 2015 after this number of articles has increased. This low amount of research further enforces the need for research.

1.5 Contribution

While additive manufacturing is already used in production, the efficiency can still be improved by utilizing more of the build chamber volume. It is important to research ways to make AM more efficient. Results of this thesis are important for designers who are considering utilizing metal PBF machine for large parts or larger batch sizes. Results of this thesis will be also utilized by research group of laser material processing and additive manufacturing in LUT University in further studies relating to metal additive manufacturing.

1.6 Research methods

For this thesis, a literature review and simulations will be conducted.

This thesis utilizes following types of sources for literature review:

1) books,
2) conference publications and
3) research reports.

To ensure reliability, literary sources are from 2015 onwards and peer reviewed. Checking validity is quite difficult as there is not much information on the topic of stacked metal AM builds. Because of this and similarities with large builds, sources describing large builds are considered valid. Overall, the literary sources will be used to gain a basis on which to evaluate the simulations results. Knowing how L-PBF works is critical for understanding the simulation results and creating suggestions on how to improve the results.

Simulations were done using 3DExperience which is a software developed by Dassault Systémes. Multiple simulations will be made with different geometries and stack amounts. Simulation results of the benchmark builds will be compared to the stacked ones in order to evaluate the results. The details of simulations are described in-depth in chapter 4.

2 LITERATURE REVIEW

Multiple types of manufacturing defects in metal PBF have been researched over the years. This chapter reviews most common types of defects and how they may affect stacked builds.

2.1 Defect formation

There are multiple types of possible defects in metal PBF. The most common types of defects are distortions caused by thermal stresses, porosity, and cracking. L-PBF is very prone to defects unless properly optimized for the build material. As laser melts the desired parts of the powder layer the build experiences rapid heating and cooling cycles causing stresses in the part. This along with the characteristics of powder create an environment that is very susceptible to defects (Choo et al. 2019, p. 2; Yang et al. 2018, pp 599-600)

2.2 Thermal distortions

In L-PBF, heat is mostly conducted through the solid material including built objects and supports. This causes uneven cooling in larger and stacked builds when comparing the top and lower parts of the build. Cooling rate can be improved by using supports as heat conducts. Supports can be topologically improved for heat conduction (Malekipour et al. 2018. p. 19). Figure 3 shows how tilting of a part can affect heat input per layer.

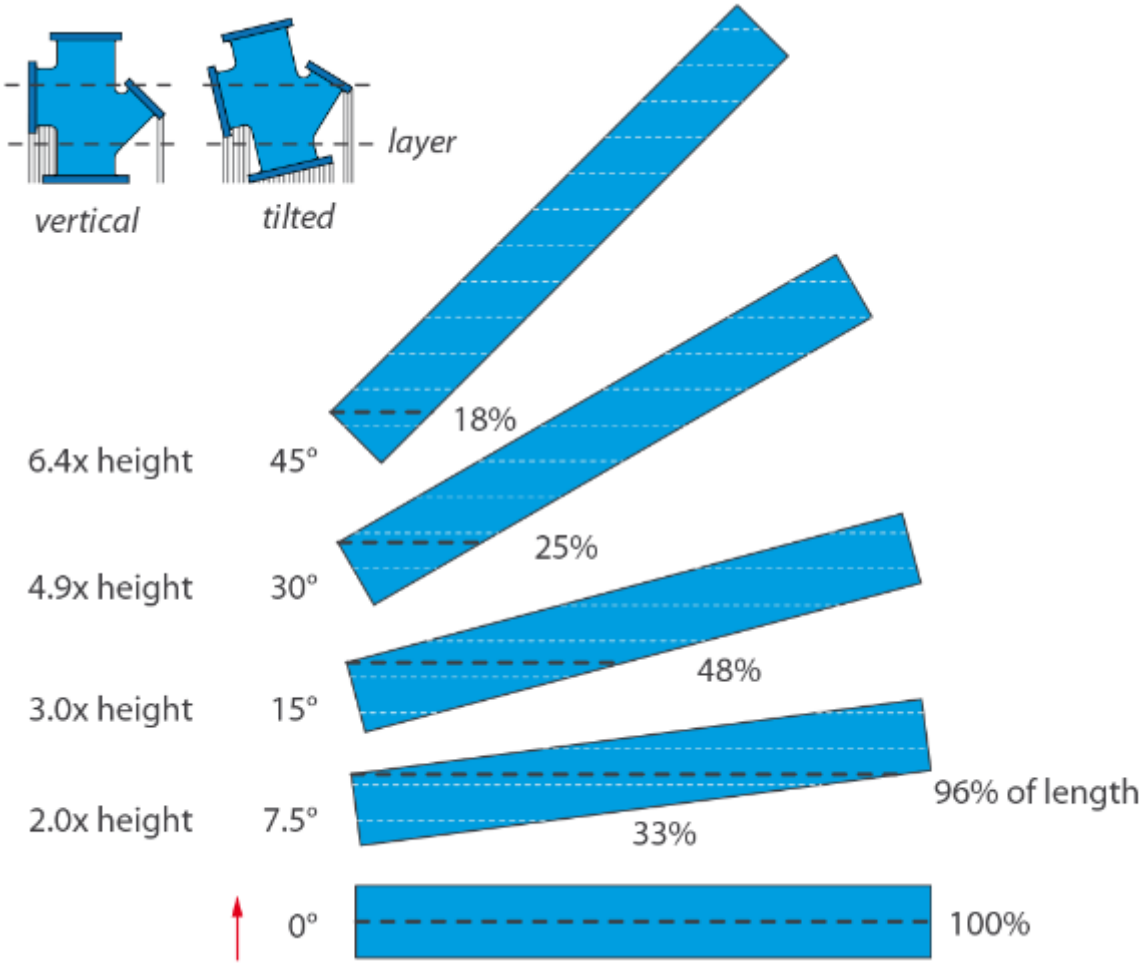

Figure 3. Effects of part tilting on heat input per layer (Kokkonen et al. 2016, p. 16). The length of the lasers path per layer is marked as a dashed line and presented as percentages.

As seen in Figure 3 (Kokkonen et al. 2016, p. 16), tilting has a significant effect on the amount of heat per layer. The amount of heat introduced to each layer is based on the length of the lasers path per layer. Build angle marked in Figure 3 is in degrees and length of the lasers path per layer is marked with the dashed line and in percentages. In the figure the heat input per layer is 100% at 0-degree angle. When tilted to a 15-degree angle the heat input per layer is down to 48%. In other words, the length of the lasers path per layer decreases when the build is tilted. Tilting reduces the heat input per layer by reducing the melted area per layer helping the build cool down between layers. Depending on the geometry of the build, tilting should be considered to reduce heat input and improve surface quality if the tilting makes the surface straight along the build direction. (Kokkonen et al. 2016, p. 16)

2.3 Residual stresses

Due to the rapid cycling of heating and cooling, L-PBF creates residual stresses to the parts (Masoomi et al. 2017, p. 75). Residual stresses occur in L-PBF when the part cools down, much like in welding. These stresses can cause distortions, cracking and delamination in the part (Brandt 2017, p. 64; Choo et al. 2019, p. 2). Different sources prove that mitigating residual stresses can be done in multiple different ways. Proper support structuring along with choosing scanning directions can be used to mitigate residual stresses (Masoomi et al. 2017, p. 75). Another way of reducing residual stresses, during the build, is to choose chessboard strategy for the lasers scan path and using supports to convey heat (Gouveia et al. 2020, p. 9).

2.4 Optimization of geometries

Geometry has a significant effect on build quality and chance of defects. Overhangs, holes, channels, or other design details can cause deformations if not addressed. Sharp corners in overhangs should be taken into consideration by using fillets. The builds can support themselves if the build angle is steeper than 45 degrees (Kokkonen et al. 2016, p. 12). Effect of build angle is visualized in Figure 4 (Kokkonen et al. 2016, p. 12).

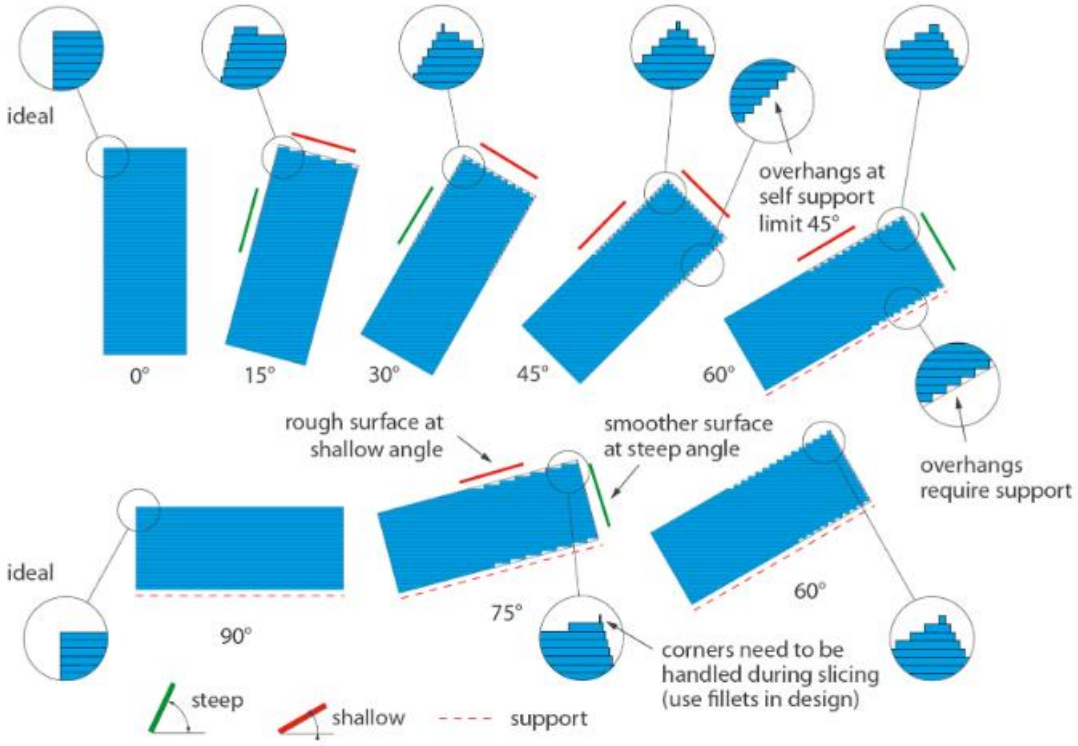

Figure 4. Build angle limitations and effects in L-PBF (Kokkonen et al. 2016, p. 12).

The builds can generally support themselves when the build angle is steeper than 45 degrees. This limit angle is also visualized in Figure 4 (Kokkonen et al. 2016, p. 12). Tilting of rectangular shape will affect the surface roughness of the build, but it will reduce the heat input per layer as previously mentioned in chapter 3.2. Dross formation occurs in overhangs when the previous layer does not provide enough support for the new layer. This causes the new layer to sink into the powder bed. Kokkonen et al. suggests using supports after the limit angle has been reached to prevent dross formation. The limit angle is not a set value, as process parameters and material properties affect it. (Kokkonen et al. 2016, p. 17-22)

2.5 Microstructure and porosity

Microstructure of metals is defined by cooling rate and processing while cooling. Microstructure formation can be controlled by the process parameters (Choo et al. 2019, p. 2). Thermal history of the manufactured part is locally dependent and can cause local differences in the microstructure (Adegoke et al. 2020, p. 2). In the case of AlSi10Mg the mechanical properties are heavily dependent on the microstructure of alloy along with porosity (Gouveia, et al. 2020, p. 2). Porosity is an issue when manufacturing parts with AM

technology. Porosity can be formed by gas entrapment, improper layering, and incomplete melting. Porosity caused by incomplete melting is less prevalent when the volume energy density (VED) is increased (Choo et al. 2019, p. 2). Sanaei et al. suggest that defect characteristics have impact on mechanical properties of parts. With SLM H13 steel porosity will not cause significant effect on fatigue resistance if pores are kept small and evenly distributed (Kokkonen et al. 2016, p. 84-86). Thermo-mechanical processes and surface treatments can be used on AM parts to improve microstructure. Hot isostatic pressing (HIP) can be used to decrease the size and amount of defects, along with improving microstructure and strength/fatigue properties of parts. (Sanaei et al. 2019, p. 3.)

2.6 Machining

Machining is one of the post processing methods used to improve additively manufactured parts. As the surface quality of AM products can be rough, machining can be used to improve the quality of the surface. Machining can be used to remove material in such a way that a geometrical tolerance will be achieved. Some aspects that need to be taken into consideration

when designing machining tolerances are presented in Figure 5 (Kokkonen et al. 2016, p. 84).

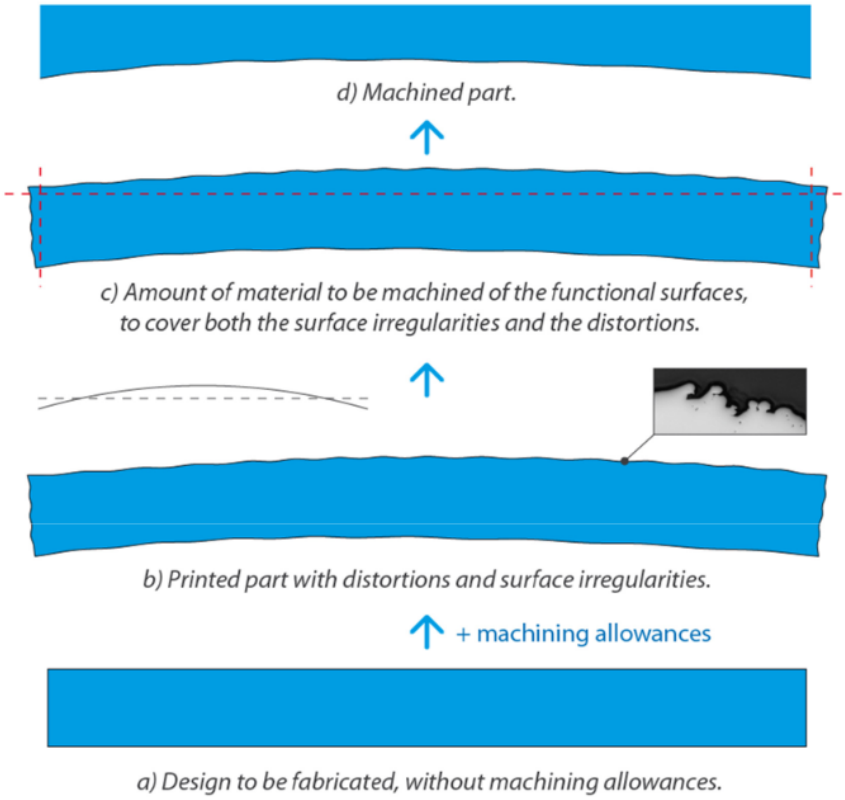

Figure 5. Effects that need to be taken into consideration when assessing machining allowances (Kokkonen et al. 2016, p. 84).

As seen in Figure 5, multiple different irregularities and geometrical distortions should be taken into consideration when defining machining allowances. Additional allowances may be needed for geometrical deviations. Surface irregularities also include subsurface porosity and dross. Functional surfaces may require larger machining allowances. (Kokkonen et al. 2016, p. 80-84.)

2.7 Simulations and distortion compensation

Stresses and deformations are one of the interesting aspects of the AM process and predicting their formation can be done using simulation. Conduction heat transfer models are a common way of simulating L-PBF of metals (Bayat et al. 2019, p. 214). L-PBF can be simulated with finite element (FE) method, using thermo-mechanical or inherent strain method. The main

difference between these two methods is that thermo-mechanical method either uses FE thermal analysis or analytical temperature field that is then used to calculate the resulting stresses and deformations. A moving heat source is commonly used for simulating the laser in thermo-mechanical models (Bayat et al. 2020, p. 2). Inherent strain method ignores thermal evolution and uses anticipated thermal values instead. Both methods allow for the calculation of stresses and distortions that are present in the L-PBF process. (Yaghi et al. 2019, pp. 224–225)

Distortion compensation using finite element analysis (FEA) is a procedure where a FE distortion prediction is used to create a new model that compensates for the distortions that happens during manufacturing. Model creation is done by inverting the predicted displacements and changing the mesh coordinates. The new model is predistorted in such a way that the end distortions should be compensated resulting in reduced distortions. (Yaghi et al. 2019, pp. 230–234; Afazov S et al. 2017, pp. 20)

3 EXPEREMENTAL METHODS

Simulations were done using Dassault Systémes 3DExperience software. As the geometry of parts were already available the parts did not need to be designed in the 3DExperience part designer. Instead the parts were imported from Autodesk Inventor Professional 2019. All the simulation work was done using the simulation software apart from part creation.

3.1 Simulation software

The simulation software is 3DExperience that is developed by Dassault Systémes. The software has capabilities for marketing, mechanics, and other applications. The applications used in this work are the “Powder Bed Fabrication App” and “Additive manufacturing scenario App”. Powder bed fabrication application was chosen as that is used to define the process parameters for the L-PBF process. Additive manufacturing scenario app is used for other parameter definitions such as mesh size. The parameter definitions are described in chapter 3.3.

3.2 Simulated geometries

Two different types of objects were simulated. First object is a tensile test rod based on the SFS standard 3471. The second object is a half-arc that will be presented later in this chapter. The rod is represented in Figure 6.

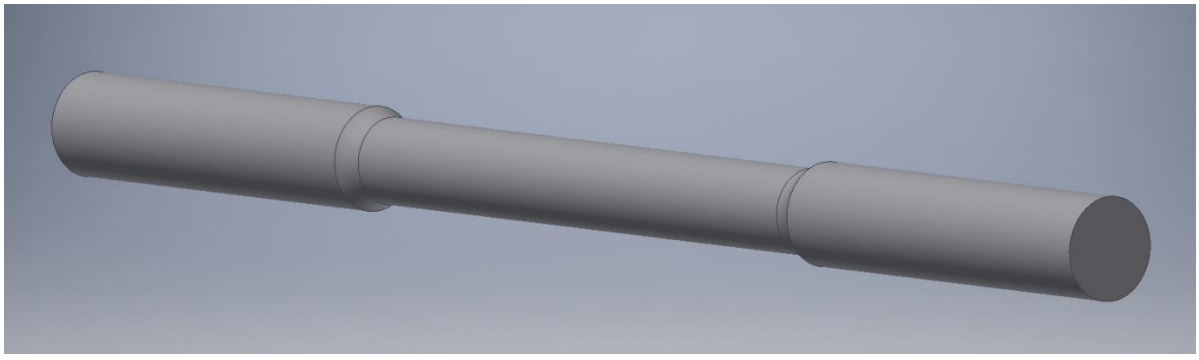

Figure 6. Three-dimensional view of rod in CAD environment.

Three-dimensional view of the rod in Autodesk Inventor 2019 Professional CAD software. Take note of the filleted inner edges of the thinner part of the rod. Dimensions of the rod are presented in Figure 7.

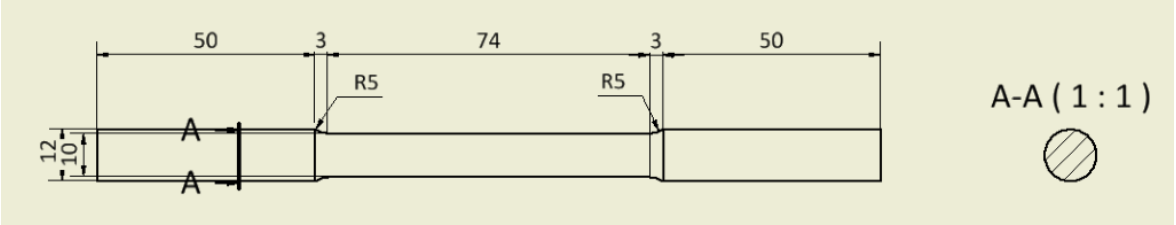

Figure 7. Rod drawing with dimensions in mm in accordance with SFS standard 3471.

As seen in Figure 7, the length of the rod is 180 mm in length and diameter is 10 mm at the middle and it follows the dimensions of SFS standard 3471. The other simulated object called half-arc is shown in Figure 8.

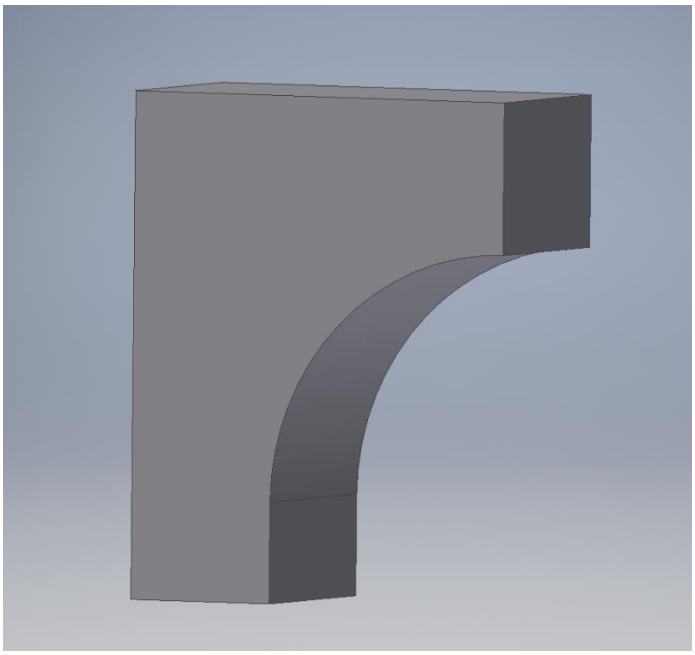

Figure 8. Half-arc in Autodesk Inventor Professional 2019.

Figure 8 illustrates how the half-arc looks like in Autodesk Inventor 2019 Professional CAD software. Dimensions of half-arc are presented in Figure 9.

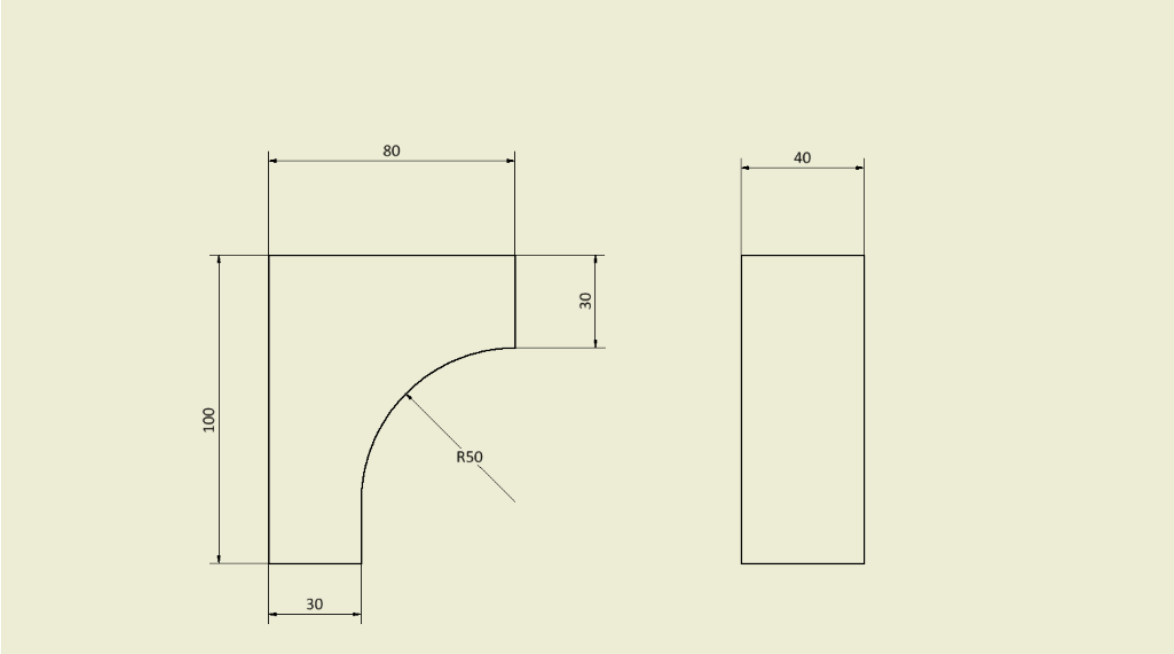

Figure 9. Half-arc drawing with dimensions.

Figure 9 shows dimensions of the half-arc. Each of these objects are going to be simulated as a single build, a double stacked build, and a triple stacked build. The half-arc is not dimensionally based on any previous research, but a similar shape has been used in previous research by Kokkonen et al. (2016). The main reason for simulating such a shape is to test how overhangs behave when stacked. There will be no supports under the overhang to maximize displacements. The rods are simulated to test how a long, but relatively thin object behaves when stacked on their side.

3.3 Simulation definition steps

The simulations require multiple steps before the actual simulations can be done. The steps mostly consist of defining parameters, supports and orientating the part. The general steps required for simulating L-PBF in 3DExperience are described in this chapter. Parameter definitions are done in the simulation software. Most relevant simulation parameters are shown in Table 1. As simulating stacked build has not been very common so the simulation parameters cannot truly be optimized for stacking. Consistency between simulations was deemed more important for proper evaluation of results.

Table 1. Most relevant simulation parameters.

Material	EOS MS1
Laser power	285 W
Scanning speed	0.95 m/s
Layer thickness	0.1 mm
Meshing type	Tetrahedron
Meshing size	1 mm

Table 1 shows the most relevant simulation parameters. The full simulation parameters can be seen in Appendix 1. All simulations use the same parameters excluding the size of the build tray. The steps required for simulating L-PBF using 3DExperience is described next.

Machined parameters are set using the "Powder Bed Fabrication App". Build chamber dimensions and laser parameters are included in the machine parameters. These parameters along with other parameters are available in detail in appendix 1. After machine parameters have been defined, the simulated objects need to be imported into the software. The imported part needs to be set and oriented onto the build chamber floor. The parts can be placed straight on the build chamber floor, but in most cases in these simulations the parts are on top of supports. The supports are wired support structures as 3DExperience does not have any other support types. A grid pattern was used for the support generation. The support structures were automatically defined by the program. A scan path generation is required for the simulations. Scan path generation needs rulesets to be defined. The parameters that these rulesets are define with can be seen in appendix 1. The scan path type is continuous.

FEA requires meshing to work. Meshing is done in the "Additive manufacturing scenario app". Meshing is dividing the part into small components. Mesh size can be set by the simulation software allowing tailored solutions for each part. Generally, larger mesh sizes result in less accurate results, but allows simplification of the model. Model simplification is done to reduce simulation time. In the simulations of this thesis all simulations use the same parameters making each result comparable with each other. Both the part and supports need to be meshed along with the build platform. After meshing both the parts and the supports, supports need to be tied to the build platform. Material that was used is EOS MS1. The material parameters were manually defined into the 3DExperience as in its current

version it does not have an AM materials database. The analysis type is thermo-mechanical, and it requires a starting temperature to be set for all components in the build. Starting temperatures and other temperature dependent parameters are seen in appendix 1. As the thermo-mechanical analysis type is based on per layer approach, 3DExperience collects all data on a per layer basis. The data collection rate is reduced in the simulations of this thesis, to reduce the size of the data pool and to speed up the simulations. For specific data collection increments see appendix 1.

4 RESULTS AND DISCUSSION

This chapter contains the simulation results and discussion about the results. The chapter is divided into two segments each describing a different type of object. First is the test rod and then is the half-arc. In both cases the benchmark results are shown first and then the double and triple stacked versions are assessed. A general assessment is done for each type of simulated object that is found in the end of each subchapter. Each figure is marked with a deformation scale. Deformation scale implicates the multiplication of the deformations that are visually shown in the figures. The amount of deformations stays the same with all deformation scales, but the visualized deformations of the models are amplified with higher values.

4.1 Test rod simulation results

Figure 10 shows displacement of the rod. This single build will work as a benchmark for the stacked builds to be compared to.

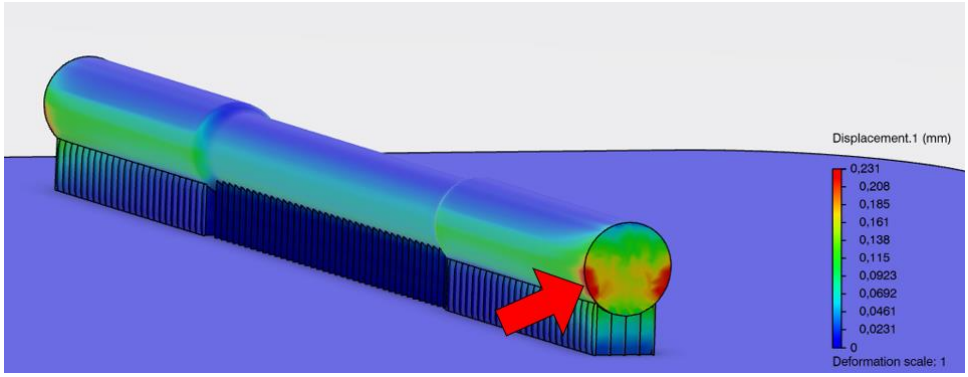

Figure 10. Displacement of rod with deformation scale 1.

As it can be seen in Figure 10, the displacement locates on the ends of the rod next to the support edges, pointed with arrow. The displacements are most likely concentrated in the arrow indicated area because the supports end in that area and do not provide the support for the part. This spike in deformation in that area could be remedied by widening the supports to cover the whole width of the rod. Figure 11 illustrates von Mises Stress of the rod.

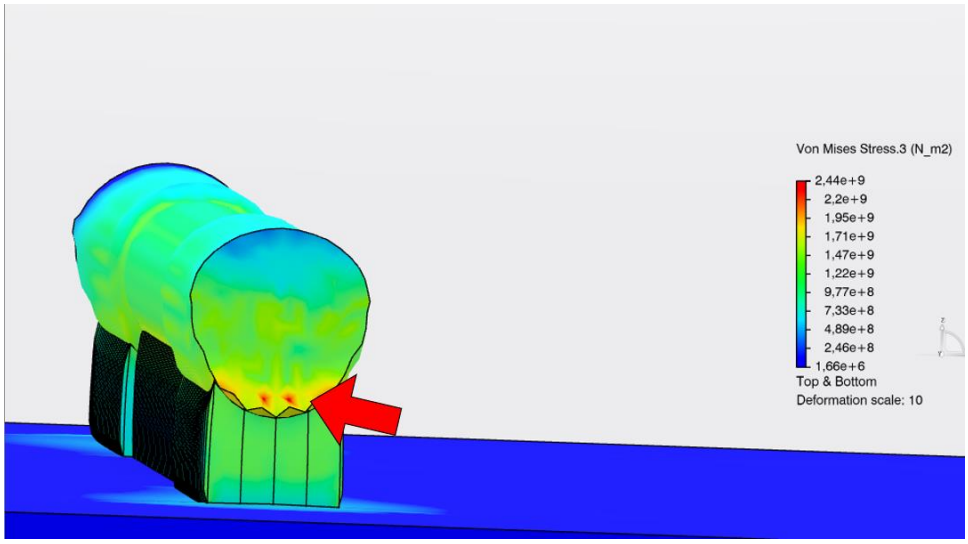

Figure 11. Von Mises Stress of a single rod. Deformation scale 10.

Figure 11 shows how stresses concentrate near the supports at the ends of the rod, pointed with arrow. The stresses have a significant of 2.44 GPa spike near the end of the rods, but apart from that the stresses are evenly distributed. Displacement of double stacked rods are presented in Figure 12.

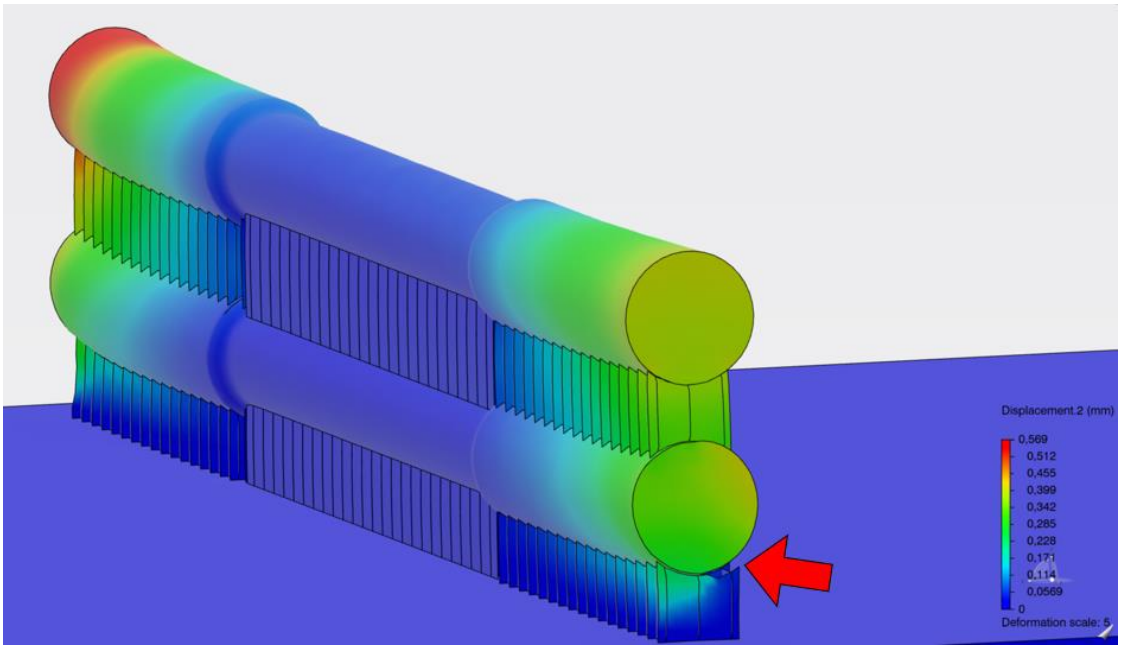

Figure 12. Displacement of double stacked rods.

Figure 12 illustrates the displacement of double stacked rods. The supports have cracked below the lower rod, pointed with arrow. Cracking is caused by thermal stresses creating a

tension in the supports that exceeds the ultimate strength of the material. Cracking could be reduced by widening the support to be the full width of the rod. Von Mises stresses are presented in Figure 13.

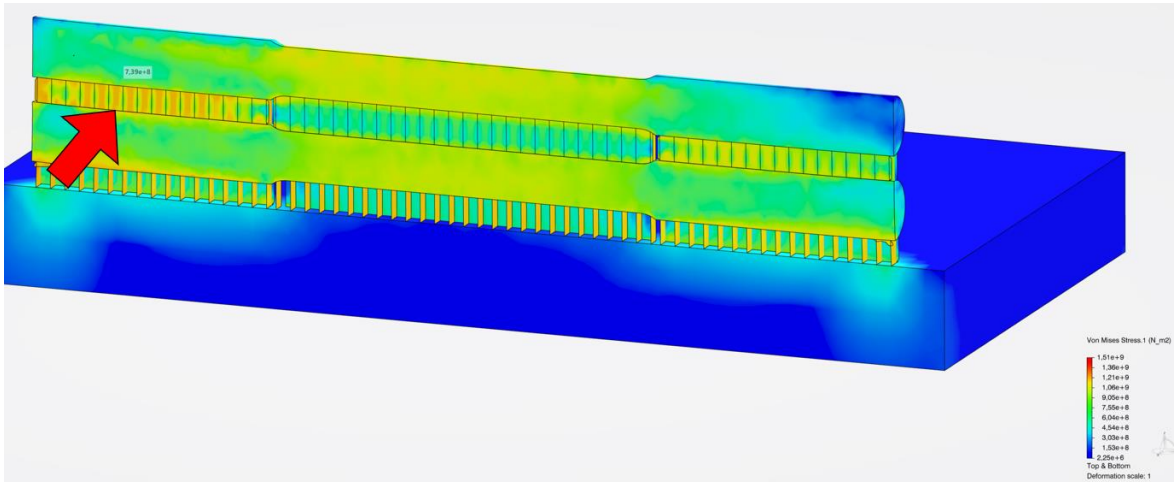

Figure 13. Von Mises stress of double stacked rods.

As seen in Figure 13, in the double stacked rods, the maximum stresses of 1.51 GPa have moved from the ends of the rods into the supports. Largest stress concentration is indicated with the red arrow. A similar concentration of stresses is not seen at the other end, but this can be explained by the temperature of the part. The indicated is the cooler one, where thermal stresses have already formed. Temperature of the double stacked rods is presented in Figure 14.

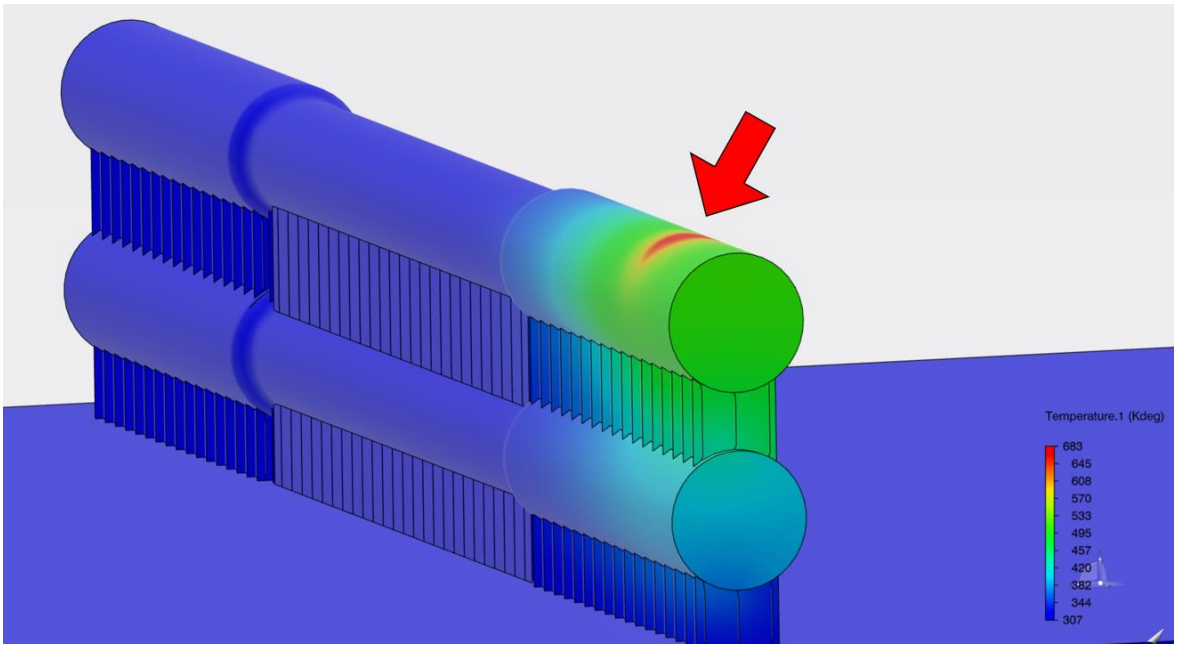

Figure 14. Temperature of double stacked rods.

Note how the temperature is not even in the build in Figure 14. The part that is still hot is annotated by the red arrow and its temperature is 683 K. The rest of the build is at 340 K. The uneven temperature is present because the simulation software does not allow the build to cool down before calculating analysis results. Uneven heat distribution causes some inaccuracies in the results as the stresses have not fully formed at this point. This could possibly be remedied with simulation parameters that would allow the build to cool down to ambient temperature. Displacements of the tiple stacked rods can be seen in Figure 15.

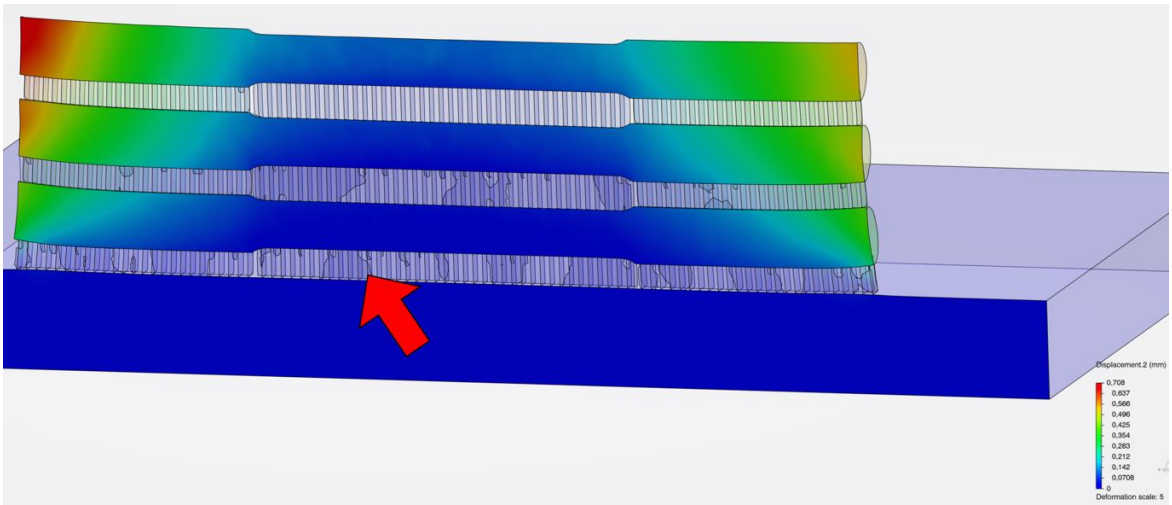

Figure 15. Test rod displacement of triple stacked rods. Half-section view.

Half-section view that is presented in Figure 15 shows that the supports seem to have some light displacement that cannot be seen from the outside. The light displacements are pointed with an arrow. The displacements are minor at around 0.142 mm. Stresses are shown in Figure 16.

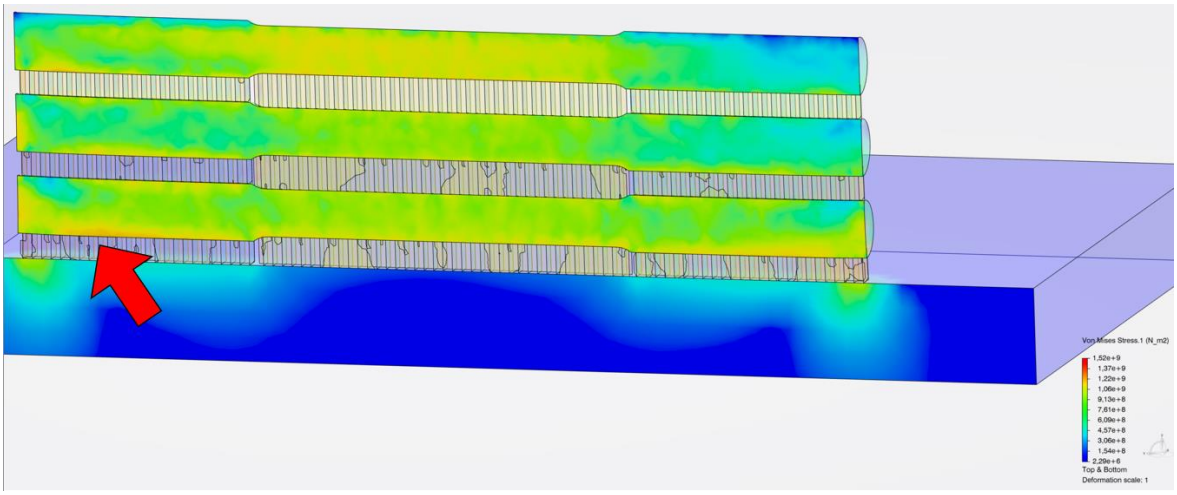

Figure 16. Test rod von Mises stress of triple stacked rods. Half-section view.

Figure 16 proves that the most significant stresses at 1.52 GPa are still concentrated in the supports of the triple stacked rod build. Stress concentration is pointed with the red arrow. This continues a pattern that was seen in previous builds. The rod itself is not under significant stress compared to the supports. Table 2 summarizes displacements of the test rods. Medium displacement is the 5th value in the displacement gradient (see appendix 2).

Table 2. Rod displacements.

Number of stacked layers	Max displacement [mm]	Medium displacement [mm]
1	0.231	0.115
2	0.569	0.285
3	0.708	0.354

As table 2 shows, the displacements increase gradually on each stack. There is a noticeable difference in the displacements between one rod and double stacked rods. A similar, but lesser difference appears between double stack and triple stack. When referencing table 2 and SFS standard 3471, it becomes clear that not all rods would be within specifications. The allowed variance within the rod body for rods with diameter of 10 mm is 0.04 mm. The benchmark rod and the lower rod in the double stack are still within specifications. Rest of the rods did not meet specifications as they had too much distortion.

4.2 Half-arc simulation results

This single object will work as a benchmark for the stacked builds. Figure 17 visualizes displacement of a single half-arc.

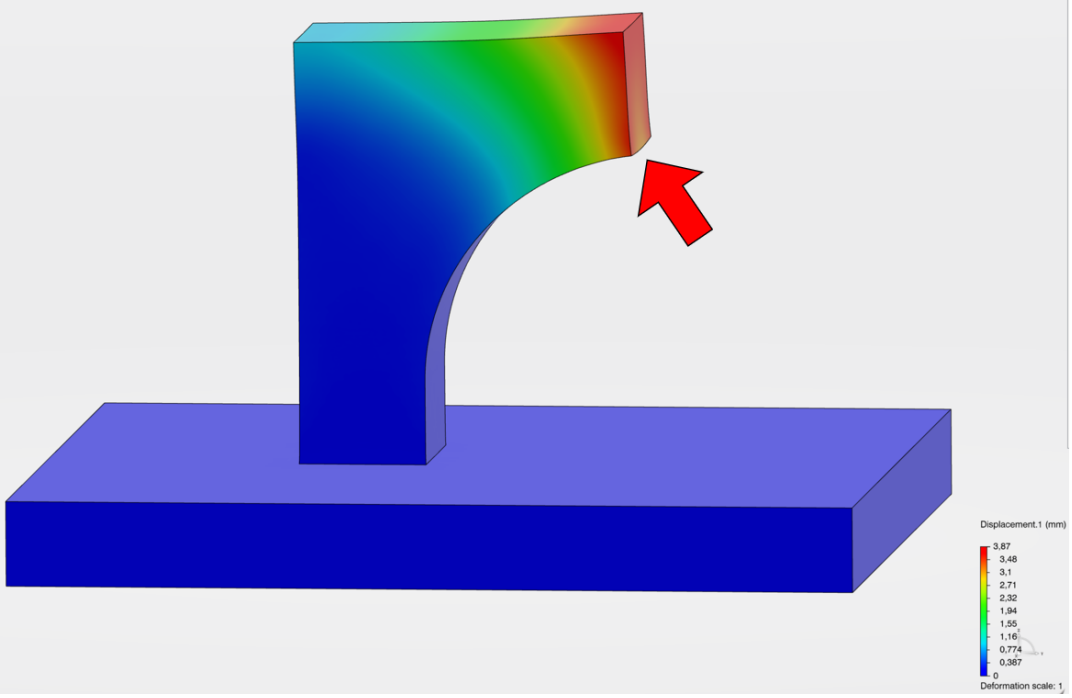

Figure 17. Displacement of half-arc. Deformation scale 1.

As seen in Figure 17, displacement of half-arc is concentrated at the end of the overhang. The overhang would cause drooping, but thermal stresses pull the edge upwards. The edge annotated by the red arrow is slightly lower from the center than the edges. The edges next to the annotated spot are also the spots which have the most deformations at 3.87 mm, pointed with arrow. Most of the build has not deformed or the deformations have been minor. These stresses are presented in Figure 18.

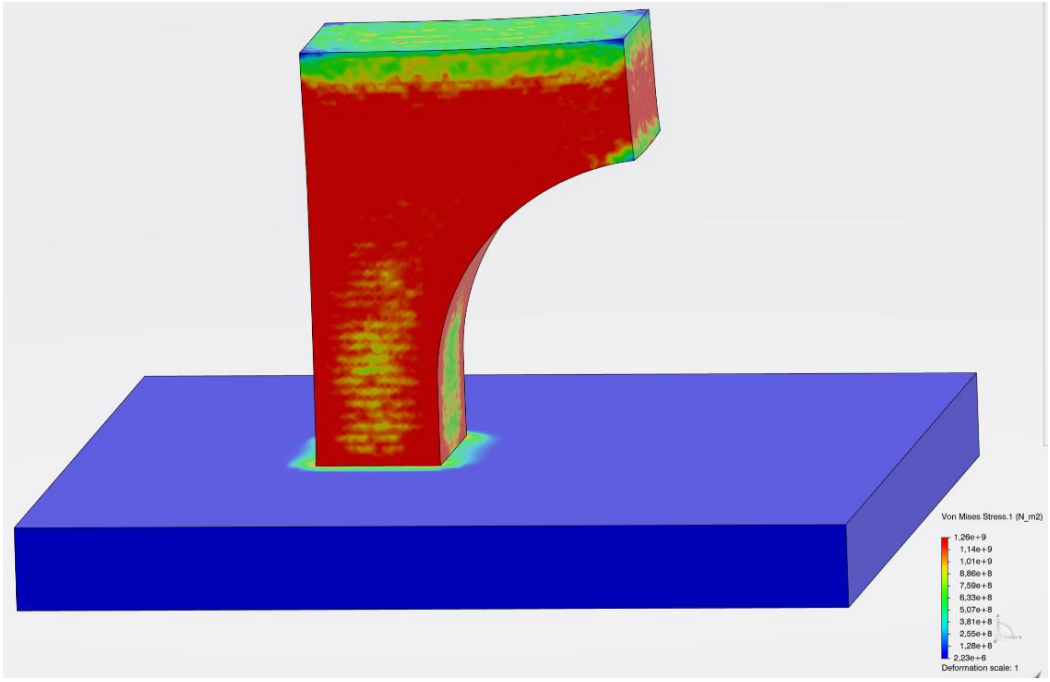

Figure 18. Von Mises stress of half-arc. Deformation scale 1.

As seen in Figure 18, stresses of the half-arc are concentrated at the edges and surfaces of the build. Although this gives a good idea on how the stresses are concentrated, this is better shown in Figure 19 in the half-section view.

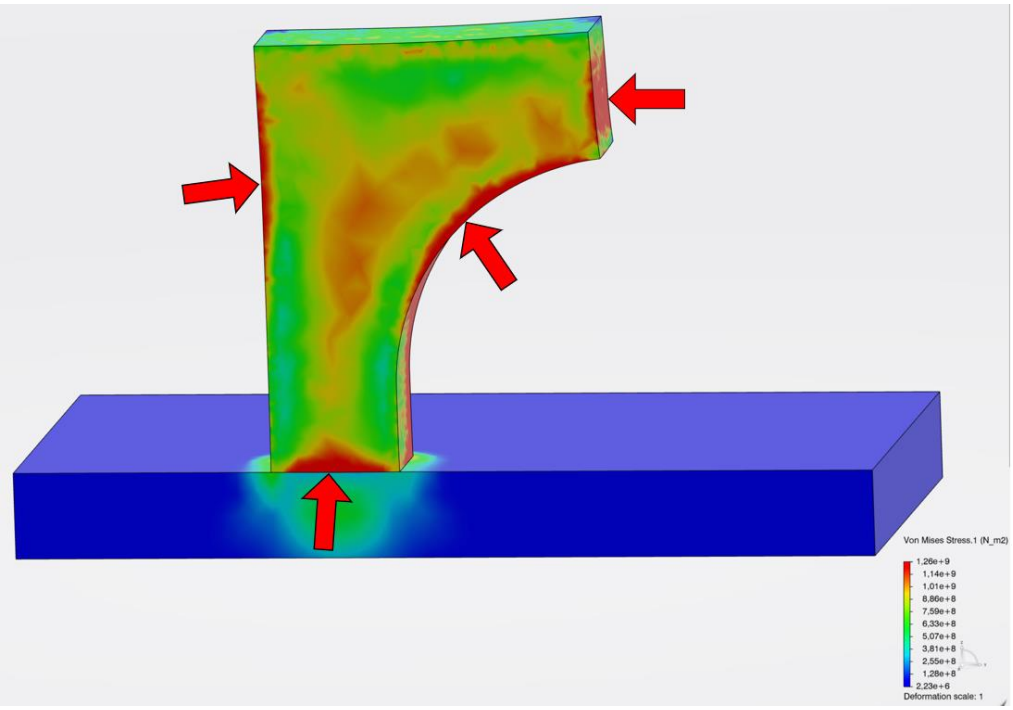

Figure 19. Von Mises stress of single half-arc. Half-section view. Deformation scale 1.

Figure 19 shows how the 1.26 GPa stresses are focused on the edges of the build as noted by the red arrows. There is also a noticeable concentration of stress in the center of the build. Displacement of double stacked half-arc is presented in Figure 20.

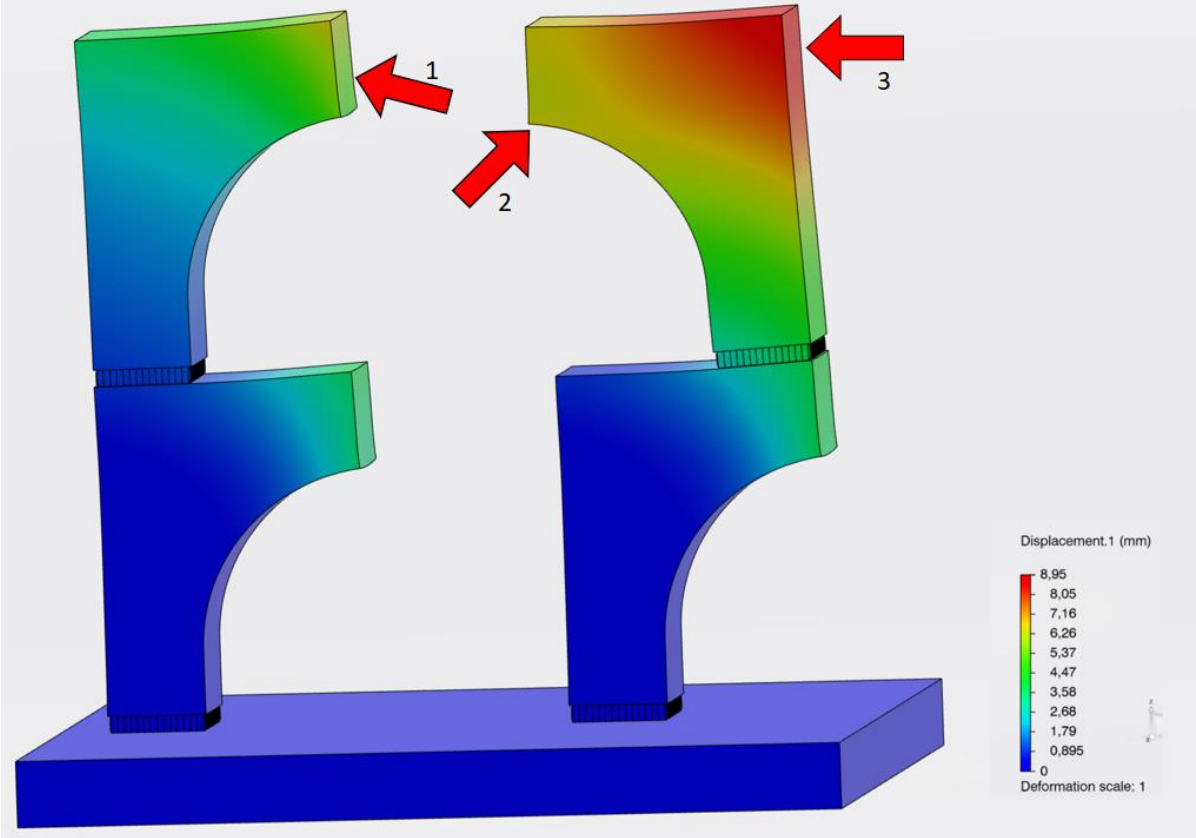

Figure 20. Displacement of double stacked half-arcs. Deformation scale 1.

As seen in Figure 20 (3), the displacement of 8.59 mm is significant. The stacking style has a clear effect on the amount of displacement. Placing the base of a build on top of the most displaced part of the previous build causes extra displacement. There is a 1 mm difference on the max deformation between the stacking styles as noted with the red arrows. The yellow color indicated displacement of 6.26 mm. As shown in Figure 20 (1. and 2.), displacement of 6.26 mm is the most displaced the less displaced stack gets. Contrasted by the more deformed part with similar displacement prevalent all over the top build. This further proves that the stacking needs to be planned in a way that the deformations will not amplify each other. Half-section view of the displacements is presented in Figure 21.

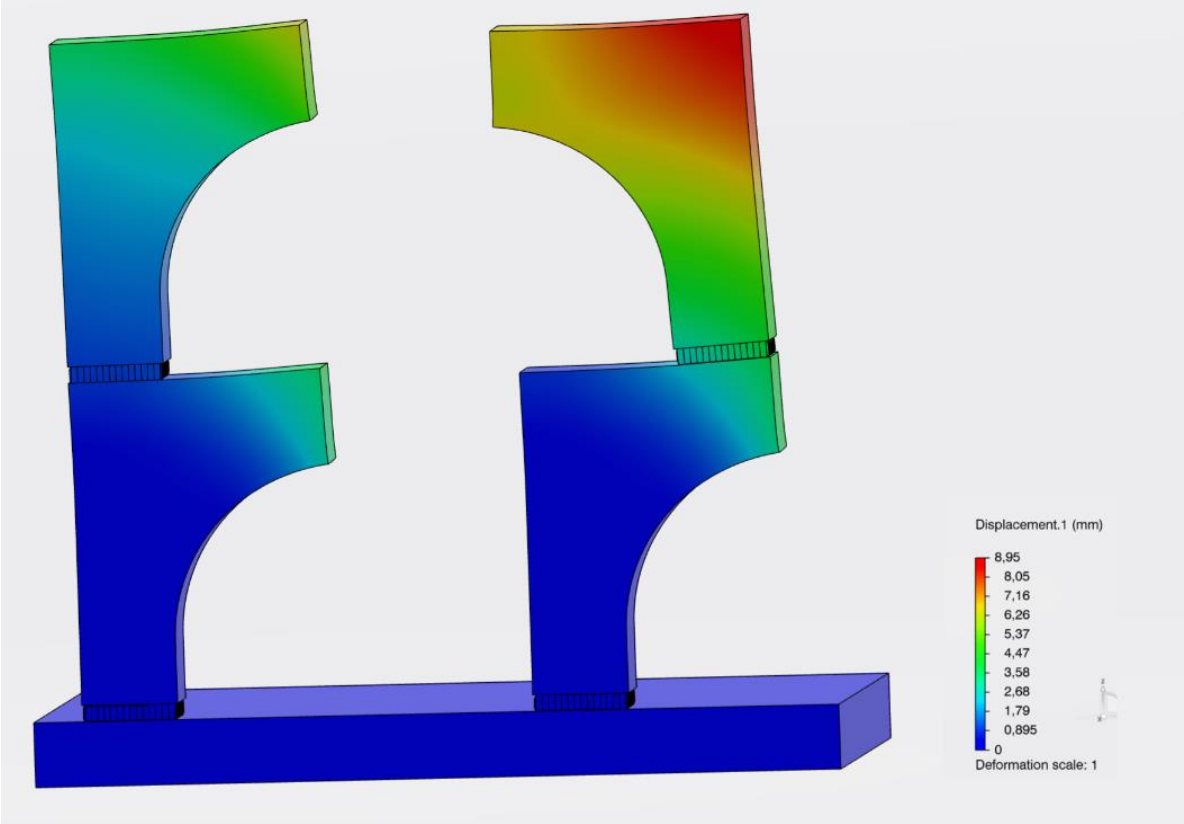

Figure 21. Displacement of double stacked half-arcs. Half-section view. Deformation scale 1.

Figure 21 shows how the displacement is similar inside the builds as they are on the outside. This is to be expected as the builds are solids inside and have no geometries inside the builds. Figure 22 shows the von Mises stresses for double stacked build.

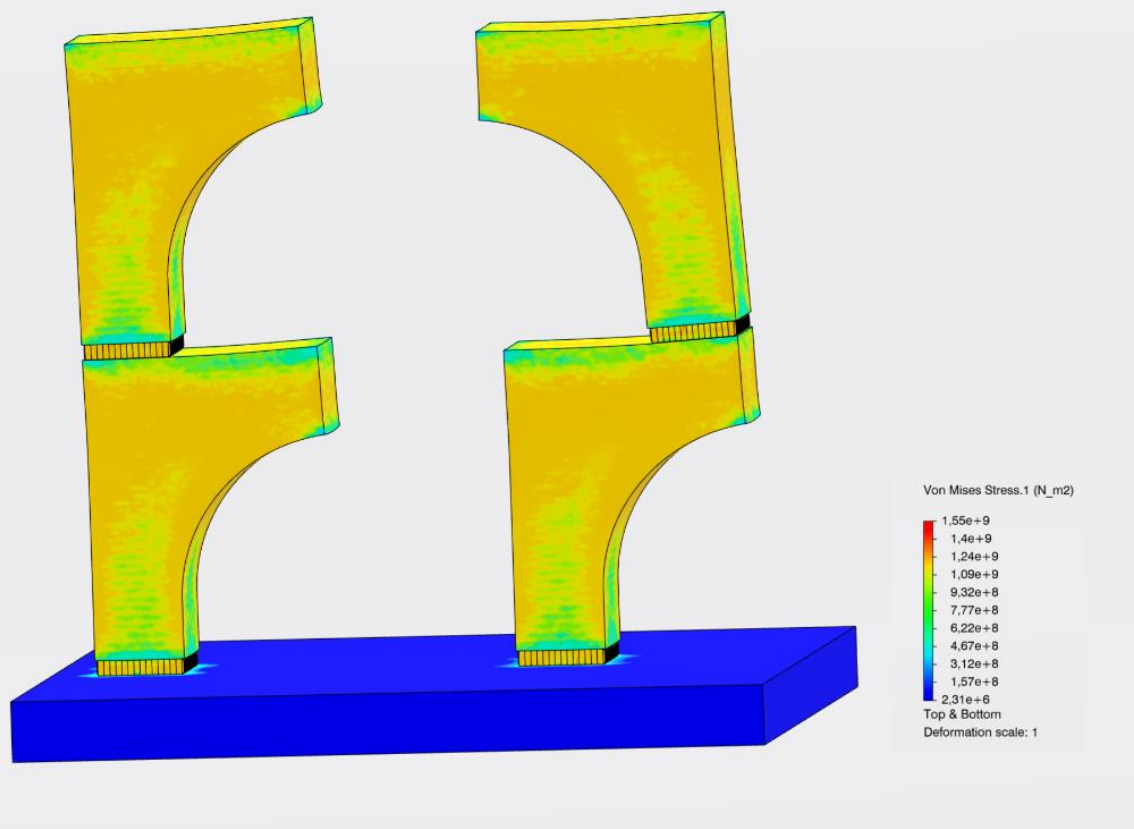

Figure 22. Von Mises stress of double stacked half-arc. Deformation scale 1.

Figure 22 proves that the stresses are near the surfaces of the build. The stress concentration is very similar to the benchmark although in the double stack the stresses are larger at 1.55 GPa. This is better seen in Figure 23 that shows a half-section view of the same stresses.

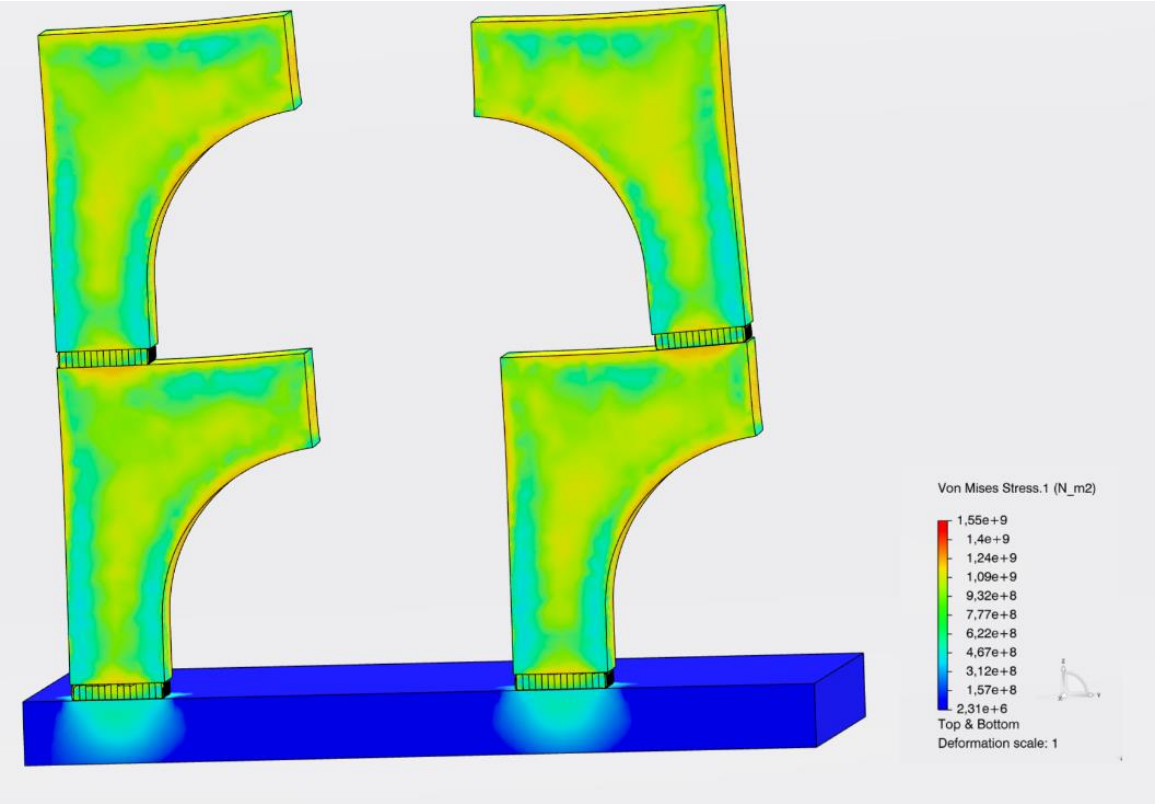

Figure 23. Von Mises stress of double stacked half-arcs. Half-section view. Deformation scale 1.

As seen in the Figure 23, the stresses are concentrated near the surfaces of the build and that there is noticeable stress concentration being conveyed by the supports. Quite surprisingly as the stack size increases, the displacements do not. Figure 24 presents displacement of the triple stacked build.

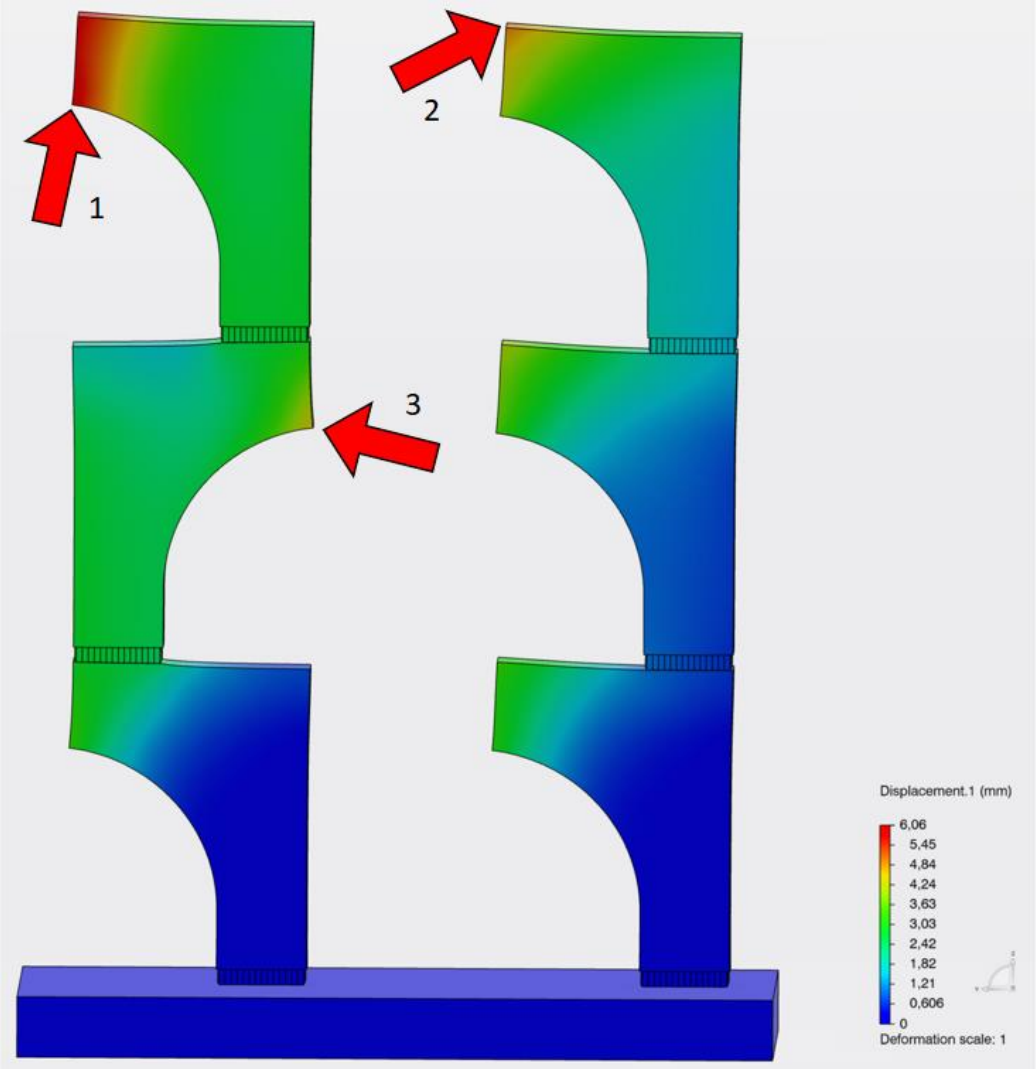

Figure 24. Displacement of triple stacked half-arcs. Deformation scale 1.

As Figure 24 shows, displacement of triple stacked half-arc parts are surprisingly lesser than in the double stacked half-arc build. The arrows indicate notable displacements in the builds. Most importantly displacement of 4.24 mm is seen in the second stack in the less advantageously stacked build whereas similar displacement is seen on the third stack of the other build as noted in Figure 24 (2 and 3). The maximum displacement is 6.06 mm and can be seen in Figure 24 (1). This is further discussed later in this chapter. Von Mises stresses are presented in Figure 25.

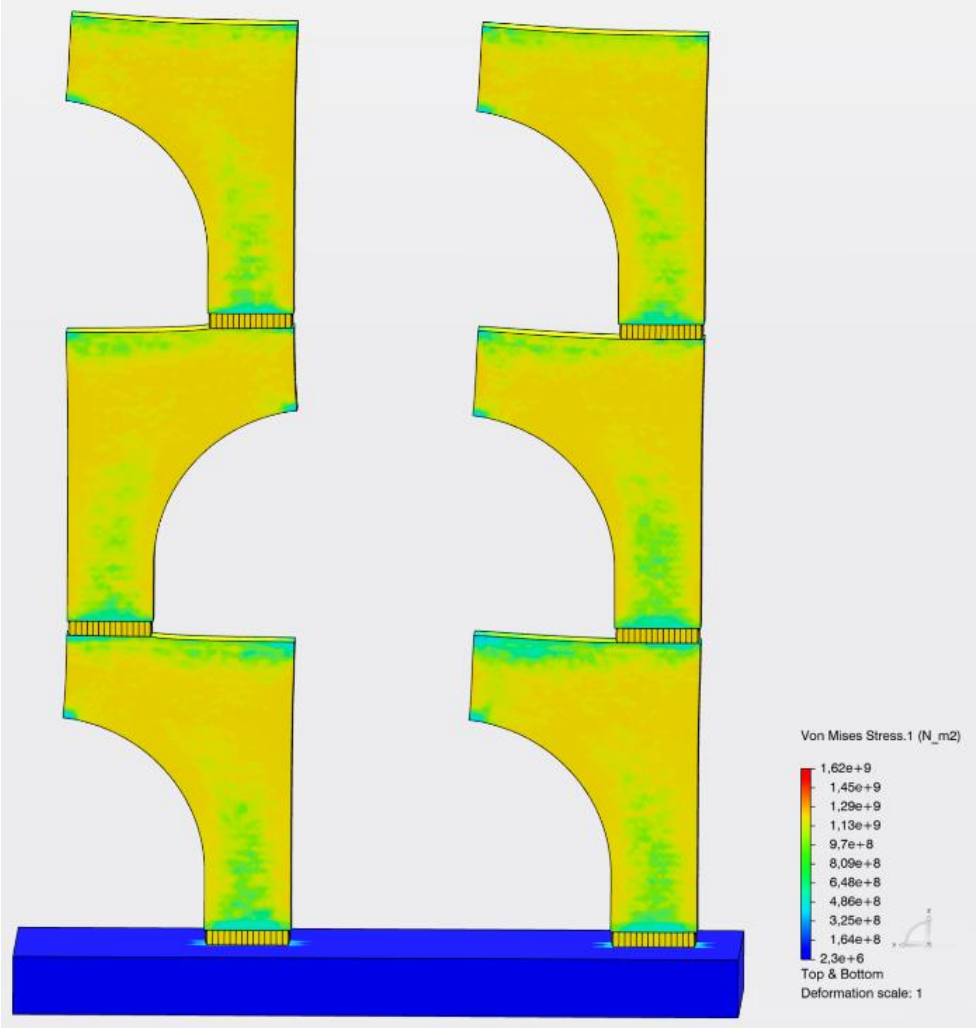

Figure 25. Von Mises of triple stacked half-arcs. Deformation scale 1.

As is the case with all the previous half-arc builds, the stresses of 1.13 GPa focus on the edges of the build as seen in Figure 25. However, in the triple stack the stresses are somewhat larger than in the previous builds. The stress concentrations are seen more clearly in Figure 26.

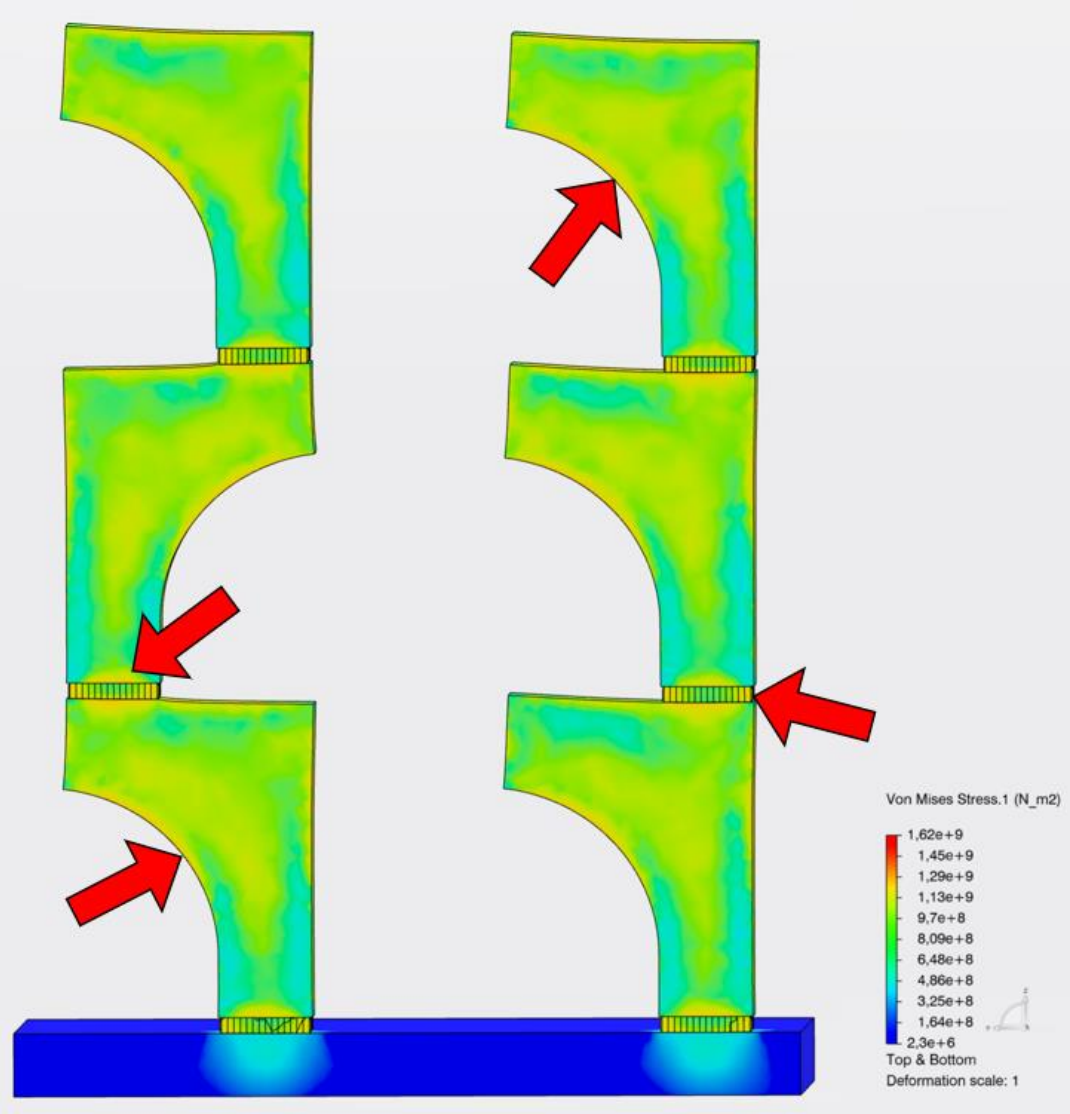

Figure 26. Von Mises stress of triple stacked half-arc. Half-section view. Deformation scale 1.

Figure 26 shows how the stresses are concentrated around the triple stacked half-arc. The stresses of 1.62 GPa are concentrated in the supports and in the overhangs as pointed by the arrows. There seems to be very little difference on the amount of stress in the overhangs between the stacking styles. Supports have a similar stress gradient between builds. Table 3 summarizes the maximum and medium displacements of all three builds. Medium displacement is the 5^{th} value in the displacement gradient (see appendix 2).

Table 3. Displacement of the half-arc builds.

Number of stacked layers	Max displacement [mm]	Medium displacement [mm]
1	3.87	1.94
2	8.95	4.47
3	6.06	3.03

Displacement is not linear with the half-arcs (see table 3). Displacement increases with the double stack but reduces with the triple stack. Compared to the displacements of the rods these displacements give a different picture of displacements in stacking. This variance in displacement requires further research to fully understand this phenomenon.

5 LIMITATIONS OF SIMULATION SOFTWARE

The first attempt at simulating stacked builds failed because the supports did not form properly due to the way the simulation program handles support building. Doing the stacking with the simulation software does not work properly. Placing a single part on the bottom and then copying others on top of it in the simulation software does not work. If stacking is done in this manner the supports penetrate and completely ignore existence of the parts below it, making the results faulty. This would be the same as simulating two separate rods, one with shorter supports and the other with taller supports. This will make the builds seem a lot less deformed than they truly are. Stacking the builds for simulation should be done in a CAD-program. This way the simulation software will recognize the parts as one and generate supports between the parts, thus accurately representing the stacking of builds. Displacement of failed stack can be seen in Figure 27.

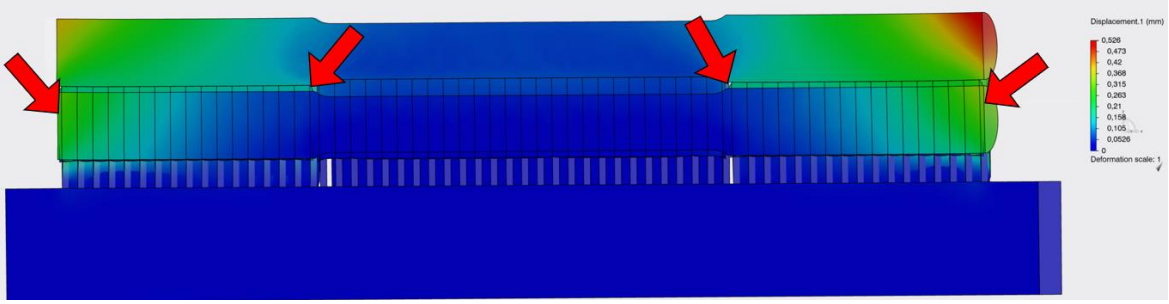

Figure 27. Failed build. Displacement, half-section view. Deformation scale 1.

As seen in Figure 27, the supports penetrate and ignore the part below it, making results faulty. The red arrows indicate how the supports penetrate the lower build. Figure 28 shows end-section view of failed build displacement.

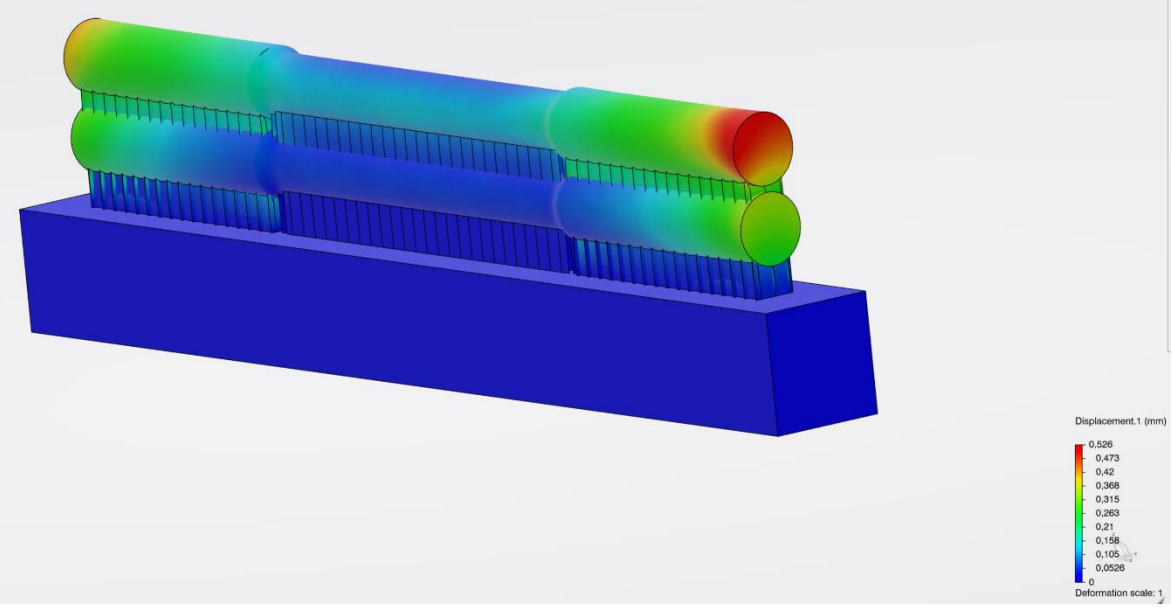

Figure 28. Failed build displacement. Deformation scale 1.

As seen in Figure 28, the support penetration cannot be seen from outside. Therefore, it is recommended to check the results with half-section views. Although maximum displacement is only marginally smaller in the failed build than in the properly simulated one, the displacement does not move as gradually. Instead the top build is more evenly displaced than in the proper builds.

6 CONCLUSION

The objective of this thesis was to study the effects of vertically stacking objects in L-PBF of metals. The meaning of this thesis was to be one of the first pieces of literature to cover the stacking of objects in L-PBF.

This thesis was executed as part of project “Metal 3D Innovations (Me3DI)”. Aim of Metal 3D Innovations (Me3DI) project is to form industrial knowhow cluster of metallic 3D printing to South Karelia. This cluster will enhance utilization of AM (3D printing) of metallic materials. The project duration is 1.9.2018-31.12.2020 and is funded by European Regional Development Fund. Cluster for metallic 3D printing gathers regional knowhow in industrial manufacturing and design and utilizes resources of academic research and education at LUT University (LUT). Thesis was written in Lappeenranta, Finland.

The literature has a clear focus on defect formation in overall applications of L-PBF. There was not any mention of stacking or vertical nesting in the literature, apart from the case studies by the commercial side. Regardless of the lack of stacking guidelines, the literary sources show that with parameter optimization, stacking will be possible. Focusing on heat input per layer and support optimization should result in better quality builds overall.

The programs used in the simulations and modelling were Dassault Systémes 3DExperience and Autodesk Inventor Professional 2019, respectively. The simulated objects were a tensile test rod and a half-arc. The objects are based on geometries commonly used in either material testing, or testing of geometrical accuracy in AM.

The results show that deformations increase when builds are stacked. The main type of deformation is bending upwards. This is caused by the heating and rapid cooling. As the new layer is heated powder particles melt and have expanded due to thermal expansion. The same expansion is also reverted as the layer cools down creating tension in the test piece. As more layers are created the build will have more tension in the top, bending the test piece upwards. Some similarities were noticed between the half-arcs and test rods. Both had increased displacements when stacked and similarly stresses were also increasing with stacking. Support generation and tilting could have been done to reduce the thermally induced stresses,

but these results are meant to be more of a benchmark for future research. This is especially relevant for the rods as they would gain the most from tilting due to their long, but thin shape. The results could not explain why the displacement increase per stack was not linear with the half-arcs.

Despite unclear results with the half-arcs, the simulation results suggest that stacking will be viable although some precautions need to be made to ensure necessary build quality. Optimization efforts need to be made to combat heat induced stresses that were the most problematic in the cases of this study. Tilting and support optimization should be considered when stacking rod-like builds. Scanning style change could be changed to see how much of a difference that makes to the distortions.

According to results of this thesis, more attention should be paid into the simulation parameters when simulations of L-PBF are carried out. The easiest way would be to lower the layer thickness to better match the true layer thickness of the builds. This increases the simulation time but creates more accurate results. Different types of simulations could also be tried to create some reference points for the accuracy between simulations.

7 FURTHER STUDIES

As the simulation software used in this study was incapable of simulating porosity in additive manufacturing, similar tests should be made with a focus on porosity formation. This is relevant as porosity formation is linked to temperatures in the build and stacked builds experience more heat as there are more layers.

Stacking requires further research as current literature has limited information regarding stacking. Too much weigh is placed on the personal experience of the operator when simulating stacked builds. More simulations and physical prototypes need to be made to make enough reference cases for further testing and possible stacking guidelines.

More studies need to be made for larger objects that are stacked as the object size may have impact on deformations when stacking builds. This could be combined with extra holes used for lessening thermal concentrations to see how much of an effect heat concentration has on build deformations.

LIST OF REFERENCES

Additive Manufacturing Today. 2018 Betatype Begins Serial Production for 3D Printed Automotive Headlight Heatsink. [Additive manufacturing Today webpage]. [Referred 16.9.2020] Available: https://additivemanufacturingtoday.com/betatype-begins-serial-production-for-3d-printed-automotive-headlight-heatsink

Adegoke, O., Andersson, J., Brodin, H., & Pederson, R., 2020. Influence of laser powder bed fusion process parameters on voids, cracks, and microhardness of nickel-based superalloy alloy 247LC. Materials, 13(17), 3770, p 2.

Afazov S., Denmark W., Toralles B, Holloway A, Yaghi A., 2017. Distortion prediction and compensation in selective laser melting. Additive Manufacturing, Volume 17, pp 15-22.

Brandt, M. (2017). Laser Additive Manufacturing - Materials, Design, Technologies, and Applications, pp 64.

Bayat M., Mohanty S., Hattel. J, 2019, A systematic investigation of the effects of process parameters on heat and fluid flow and metallurgical conditions during laser-based powder bed fusion of Ti6Al4V alloy, International Journal of Heat and Mass Transfer, Volume 139, pp 213-230.

Bayat M., Klingaa C., Mohanty S., Baere D, Thorborg J., Tiedje N., Hattel J., 2020. Part-scale thermo-mechanical modelling of distortions in Laser Powder Bed Fusion – Analysis of the sequential flash heating method with experimental validation, Additive Manufacturing, Volume 36, p 2.

Choo, H., Sham, K. L., Bohling, J., Ngo, A., Xiao, X., Ren, Y., Depond, P. J., Matthews, M. J., Garlea, E. 2019. Effect of laser power on defect, texture, and microstructure of a laser powder bed fusion processed 316L stainless steel. Materials & Design, 164, p 2.

Etteplan. Additive Manufacturing Design Case for Optimized Production. 2019. [Etteplan webpage]. [Referred on 16.9.2020]. Available:

https://www.etteplan.com/references/additive-manufacturing-design-case-optimized-production

Gouveia, R. M., Silva, F. J. G., Atzeni, E., Sormaz, D., Jorge, L. A., & António, B. P. 2020. Effect of scan strategies and use of support structures on surface quality and hardness of L-PBF AlSi10Mg parts. Materials, 13(10), 2248, pp 2-9.

Kokkonen, P., Salonen, L., Virta, J., Hemming, B., Laukkanen, P., Savolainen, M., Komi, E., Junttila, J., Ruusuvuori, K., Varjus, S., Vaajoki, A., Kivi, S. & Welling, J. 2016. Design guide for additive manufacturing of metal components by SLM process. VTT Research Report., vol. VTT-R-03160-16, VTT Technical Research Centre of Finland.

Malekipour E., Tovar A., El-Mounayri H. 2018. Heat Conduction and Geometry Topology Optimization of Support Structure in Laser-Based Additive Manufacturing. In: Wang J. et al. (eds) Mechanics of Additive and Advanced Manufacturing, Volume 9. Conference Proceedings of the Society for Experimental Mechanics Series. Springer, Cham. pp 17-27.

Masoomi M., Thompson S., Shamsaei N., 2017. Laser powder bed fusion of Ti-6Al-4V parts: Thermal modeling and mechanical implications, International Journal of Machine Tools and Manufacture, 118–119, pp 73-90.

Sanaei N., Fatemi A., Phan N., 2019. Defect characteristics and analysis of their variability in metal L-PBF additive manufacturing, Materials & Design, 182, pp 3.

Yaghi, A., Ayvar-Soberanis, S., Moturu, S., Bilkhu, R. & Afazov, S. 2019. Design against distortion for additive manufacturing. Additive Manufacturing, 27, pp. 224-235.

Yang L., Hsu K., Baughman B., Godfrey D., Medina F., Menon M., Wiener S., 2017. Introduction to Additive Manufacturing. In: Additive Manufacturing of Metals: The Technology, Materials, Design and Production. Springer Series in Advanced Manufacturing, Springer, Cham, p 21.

Yang P., Jamshidinia M., Boulware P., Kelly S. M., 2018. Prediction of microstructure, residual stress, and deformation in laser powder bed fusion process. Computational Mechanics 61, pp 599–615.

Parameters used in the simulations.

Scanning optic	**Values**
Max scan speed	7 m/s
Max scan power	400 W
Max jump speed	7 m/s
Beam	
Focal diameter	0.1 mm
Maximal defocusing length	0.1 mm
Scope	
Shape type	Rectangle
Length	300 mm
Width	300 mm
Mirror mounting point	
X	0 mm
Y	0 mm
Z	200 mm
Machine parameters	**Values**
Type	Rectangular
X Minimum	-150 mm
Y Minimum	-150 mm
Z Minimum	0 mm
X Maximum	150 mm
Y Maximum	150 mm
Z Maximum	200 mm
Scanning type	
Scan path type	Continuous
Slicing step	
Minimum	0.01 mm
Maximum	1 mm

Recoating direction	
X Direction	1
Y Direction	0
Type	Back & Forth
Recoating speed	
Minimum	0.1 m/s
Maximum	0.5 m/s
Layout rules	**Values**
Manufacturing orientation frozen	Yes
Distance between part and build tray	5 mm
Distance between part and build tray frozen	No
Minimum distance between parts	5 mm
Clearance on build tray border	1 mm
Minimum height between parts	1 mm
Nesting options	Nesting with 3D with bounding box of the part
Support rules zone type	**Values**
Ground type	Build tray
Minimal surface width	5 mm
Tolerance	0.01 mm
Surface angle	
Minimum	0 degrees
Maximum	45 degrees
Shape type	
With envelope	No
Spacing	3 mm
Radial offset	0.5 mm
Direction angle	0 degrees

Z offset to Top	0 mm
Z offset to Bottom	0 mm
Scanning rule	**Values**
Global	
Beam power	285 W
Defocusing length	0 mm
Jump speed	7 m/s
Delay after jump	0 s
Continuous	
Scan speed	0.95 m/s
Global parameters	**Values**
Slicing step	0.1 mm
Upskin	
Minimal skin width	1 mm
Number of layers	1
Restrict core by upskin	Yes
Downskin	
Minimal skin width	1 mm
Number of layers	1
Restrict core by downskin	Yes
Product	**Value**
Mesh size	1 mm
Support	
Mesh size	1 mm
Thickness	1 mm
Build tray	
Mesh size	4 mm
Build tie creation	**Values**
Create tie between body and supports/build tray	Yes

Create tie between supports and build tray	Yes
Position tolerance	0.5 mm
Starting temperature setup	**Values**
Chamber temperature	299.15 K
Build tray temperature	299.15 K
Melting temperature	1000 K
Moving heat flux	**Values**
Event series source	Manufacturing cell
Laser distribution	Concentrated
Use temperature-dependent data	No
Absorption	0.45
Material input	**Values**
Follow deformation	Yes
Source type	Built-in
Event series source	Manufacturing cell
Deposition type	Roller
Free surface heat transfer	**Values**
Reference temperature	299.15 K
Convection	Yes
Convection coefficient	18 $W/K*m^2$
Radiation	Yes
Emissivity	0.25
Temperature	**Values**
Temperature	40 C
Scale factor	1
Incrementation	**Values**
Maximum increments	10000
Time incrementation selection	Automatic
Initial time increment	500 s

Minimum time increment	1e-005 s
Maximum time increment	500 s
Incrementation	**Values**
Incrementation type	Automatic
Initial time increment	500 s
Minimum time increment	1e-005 s
Maximum time increment	500 s
Maximum number of time increments	10000
Maximum temperature change per time increment	5000 K
Maximum temperature change rate for steady state: 0 [K/s]	No
Analysis case selection	**Values**
Thermal analysis case 1	4 cores
Structural analysis case 1	4 cores

Medium and maximum displacement explained.